Electronic Supplementary Material (ESI) for New Journal of Chemistry.

Copper nanoparticles grafted on carbon microspheres as novel heterogeneous catalysts and their application for the reduction of nitrophenol and one-pot multicomponent synthesis of hexahydroquinolines

Tibor Pasinszki,[a,*] Melinda Krebsz,[a] Győző György Lajgut,[a] Tünde Kocsis,[b] László Kótai,[b]
Sushama Kauthale,[c] Sunil Tekale,[c] and Rajendra P. Pawar[c]

[a]*ELTE Eötvös Loránd University, Institute of Chemistry, Budapest, H-1117 Hungary.*

[b]*Research Centre for Natural Sciences, Hungarian Academy of Sciences, Budapest, H-1519 Hungary.*

[c]*Department of Chemistry, Deogiri College, Station Road, Aurangabad (MS) 431 005 India.*

Supporting information

[*]E-mail: pasinszki@chem.elte.hu;

Table S1: Copper containing phase composition[a], estimated average grain size of crystalline phases[b], and specific surface area[c] of carbonised resin

carbonisation		**Cu_2O**	**Cu**	**ACS[b]**	**BET[c]**
temperature, °C	time, h	%	%	nm	$m^2\ g^{-1}$
500	2	8	92	14	9
	4	6	94	15	6
	8	3	97	15	8
600	2		100	15	4
	4		100	17	3
	8		100	17	3
700	2		100	16	3
	4		100	21	4
	8		100	16	4
800	2		100	19	4
	4		100	21	4
	8		100	23	6
900	2		100	26	7
	4		100	26	8
	8		100	26	4
1000	2		100	32	4
	4		100	35	4
	8		100	35	6

[a] Cu content in at%. Determined by powder X-ray diffraction (XRD). Estimated errors for XRD are within ±5%.

[b] Average crystallite size of Cu nanoparticles in nm. Estimated using the Scherrer equation.

[c] Estimated errors are within ±3%.

Table S2: Yields and melting points of various Hantzsch's hexahydroquinolines prepared using the Cu-NP/C catalyst

Entry	**Aldehyde**	**Product**	**Yield** (%)a)	**Melting point** (°C) [Ref]
11	Benzaldehyde	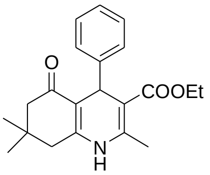	92	201-202 [1]
12	2,4-Dichlorobenzaldehyde	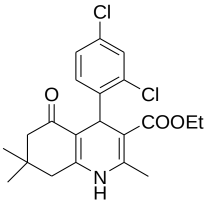	88	218-219 [2]
13	2-Chloro-4-flurobenzaldehyde	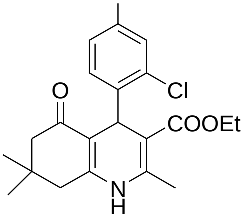	86	180-181 [present work]
14	4-Chlorobenzaldehyde	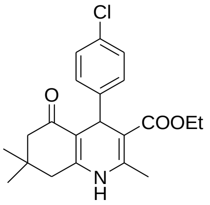	94	244-245 [1]
15	Fluorene-2-carbaldehyde	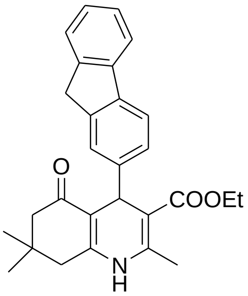	90	224-225 [present work]
16	4-Methoxybenzaldehyde	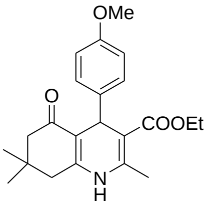	89	257-258 [1]
17	2-Hydroxybenzaldehyde	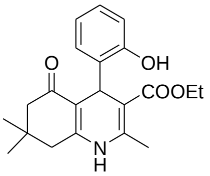	87	211-213 [3]
18	3-Hydroxybenzaldehyde	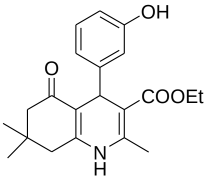	89	218-219 [4]

19	3-Nitrobenzaldehyde	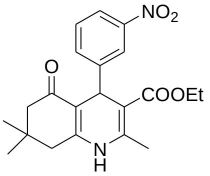	91	176-178 [1]
20	4-Nitrobenzaldehyde	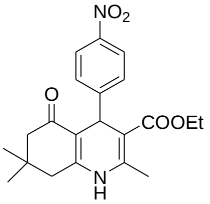	88	242-243 [1]
21	4-Bromobenzaldehyde	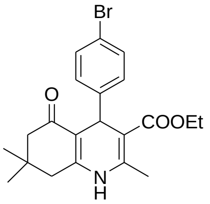	87	251-252 [1]
22	Thiophene-2-carbaldehyde	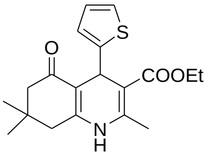	82	238-239 [1]

[a]Isolated yields for the reaction of aldehyde (2 mmol), dimedone (2 mmol), ethyl acetoacetate (2.4 mmol) and ammonium acetate (3 mmol) using Cu-NP/C (10 mg/1 mmol aldehyde) microspheres in refluxing ethanol after 2 h.

[1] M. Maheswara, V. Siddaiah, G. L.V. Damu, C.V. Rao, Arkivoc (ii), 2006, 201.
[2] B.P. Bandgar, P.E. More, V.T. Kamble, J.V. Totre, Arkivoc (xv), 2008, 1.
[3] A. Waghmare, T. Patil, K. Kadam, S. Pandit, *Iran. J. Catal.*, 2015, 5, 1.
[4] S.B. Sapkal, K.F. Shelke, B.B. Shingate, M. Shingare, *Tetrahedron Lett.*, 2009, 50, 1754.

Table S3: Catalytic activity of Cu-NP/C catalyst compared to some reported catalysts used for the four component hexahydroquinoline synthesis

Catalyst	**Rection conditions**[a]	**Yield (%), [ref.]**
$Fe_3O_4@SiO_2-SnCl_4$ (25 mg)	EtOH, reflux, 14 min	95 [1]
Glucosulfonic acid/Fe_3O_4 (50 mg)	EtOH, reflux, 240 min	90 [2]
Cu(II)-L-Histidine/Fe_3O_4 (4 mg)	EtOH, 50 °C, 95 min	92 [3]
Boehmite silica sulfuric acid (30 mg)	EtOH, reflux, 215 min	94 [4]
Cu-NP/C microspheres (10 mg)	EtOH, reflux, 120 min	92 this work

[a] Benzaldehyde (1 mmol)

[1] A. Bamoniri and S. Fouladgar, *RSC Adv.*, 2015, 5, 78483.
[2] M. Hajjami and B. Tahmasbi, *RSC Adv*. 2015, 5, 59194.
[3] M. Norouzi, A. Ghorbani-Choghamarani and M. Nikoorazm, *RSC Adv*. 2016, 6, 92387.
[4] A. Ghorbani-Choghamarani and B. Tahmasbi, *New J. Chem*. 2016, 40, 1205.

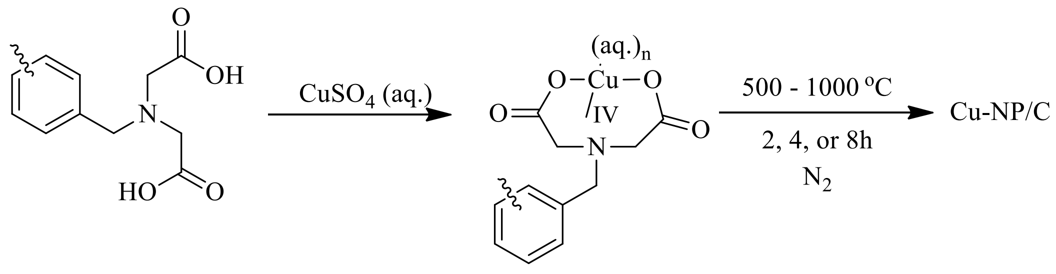

Scheme S1. Synthesis of Cu-NP/C microspheres

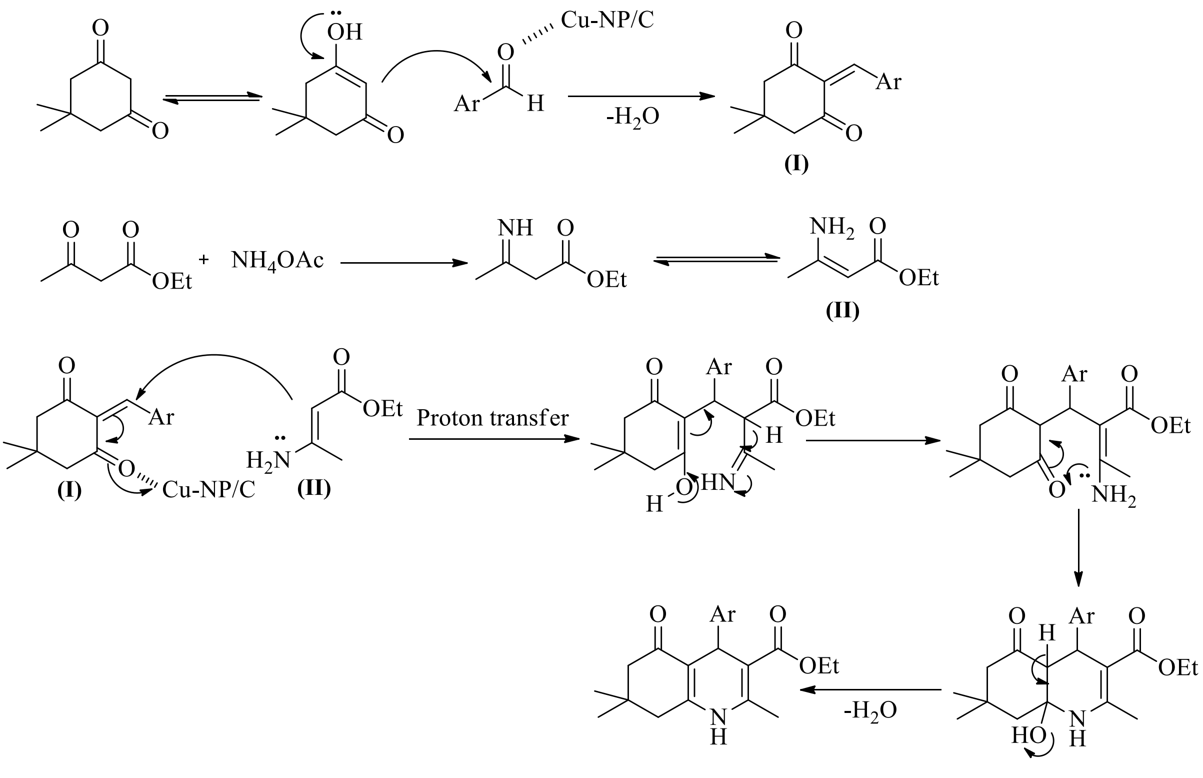

Scheme S2. Plausible mechanism for the Cu-NP/C catalyzed synthesis of Hantzsch's polyhydroquinolines

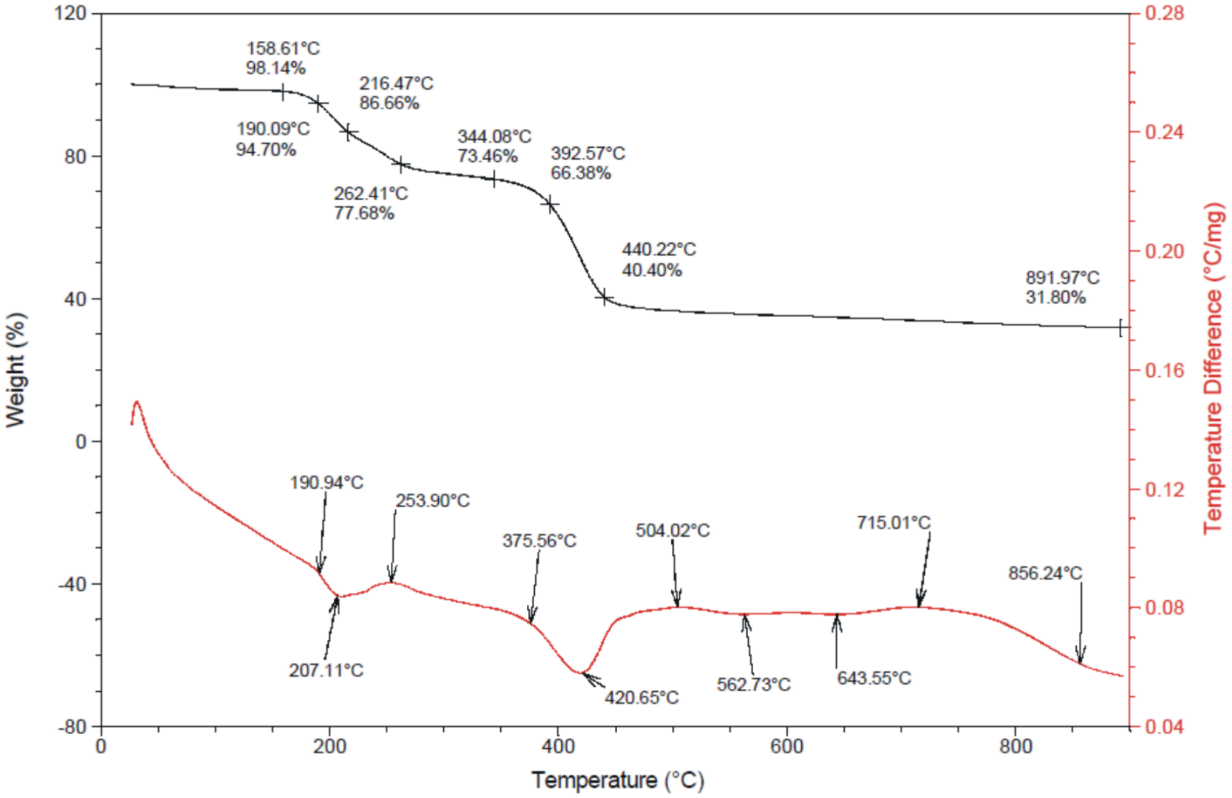

Figure S1. TGA-DTA curves of the copper-loaded ion-exchange resin

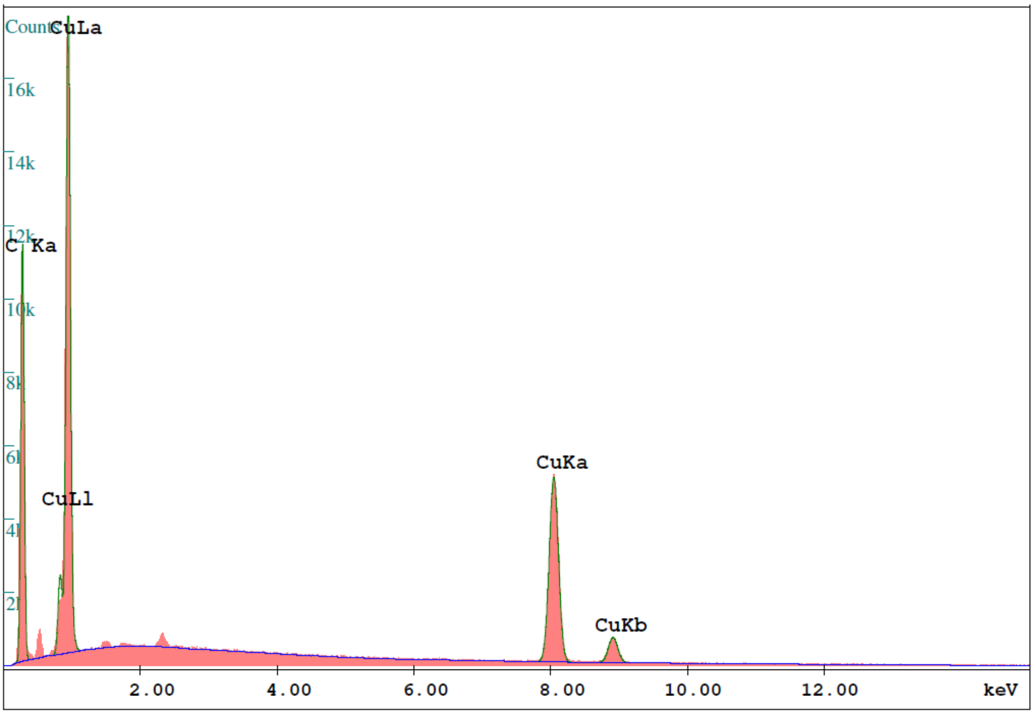

Figure S2. EDAX of the Cu-NP/C catalyst surface obtained by carbonising the precursor at 600 ºC for 4 h (C: 87 at%; Cu: 13 at%)

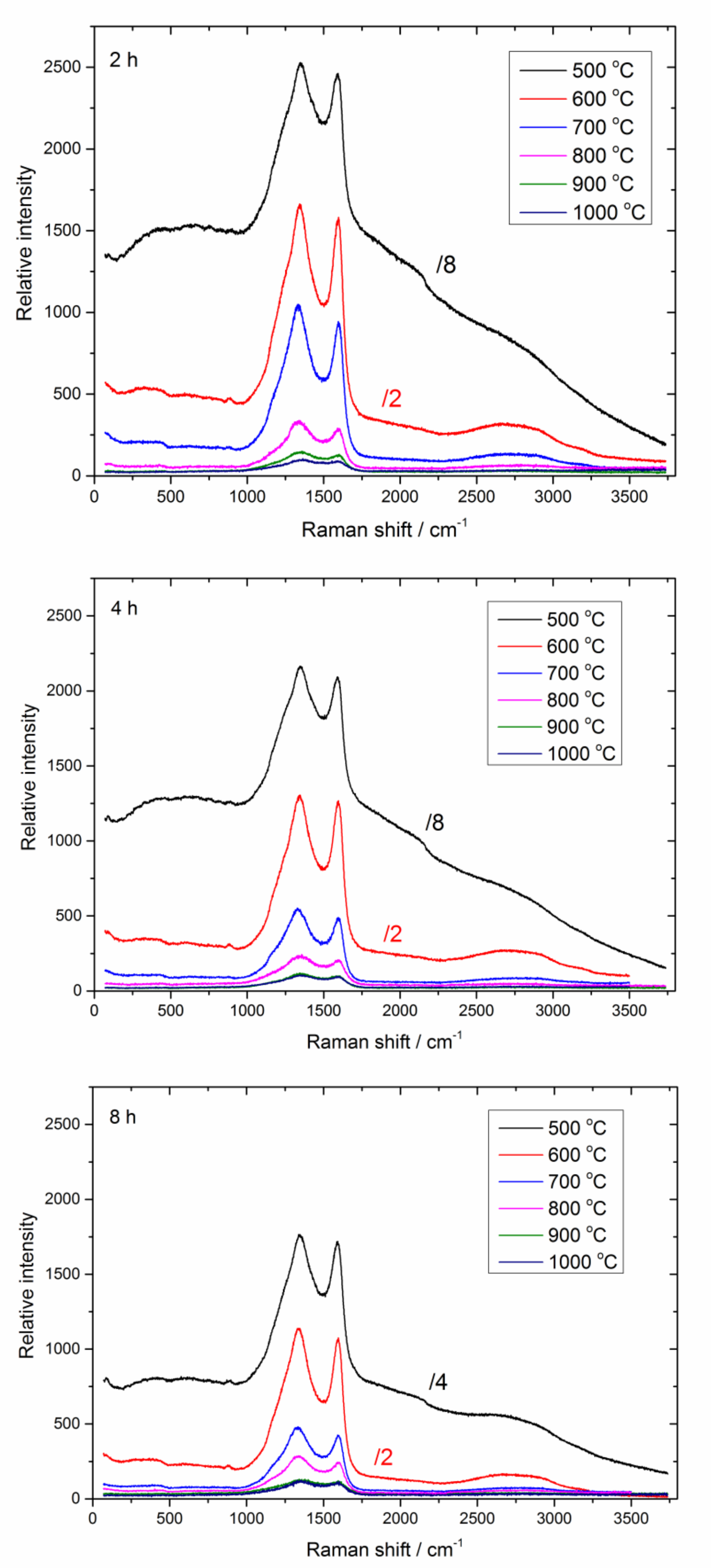

Figure S3. Raman spectra of Cu-NP/C microspheres
(Heating time and carbonization temperature are indicated.)

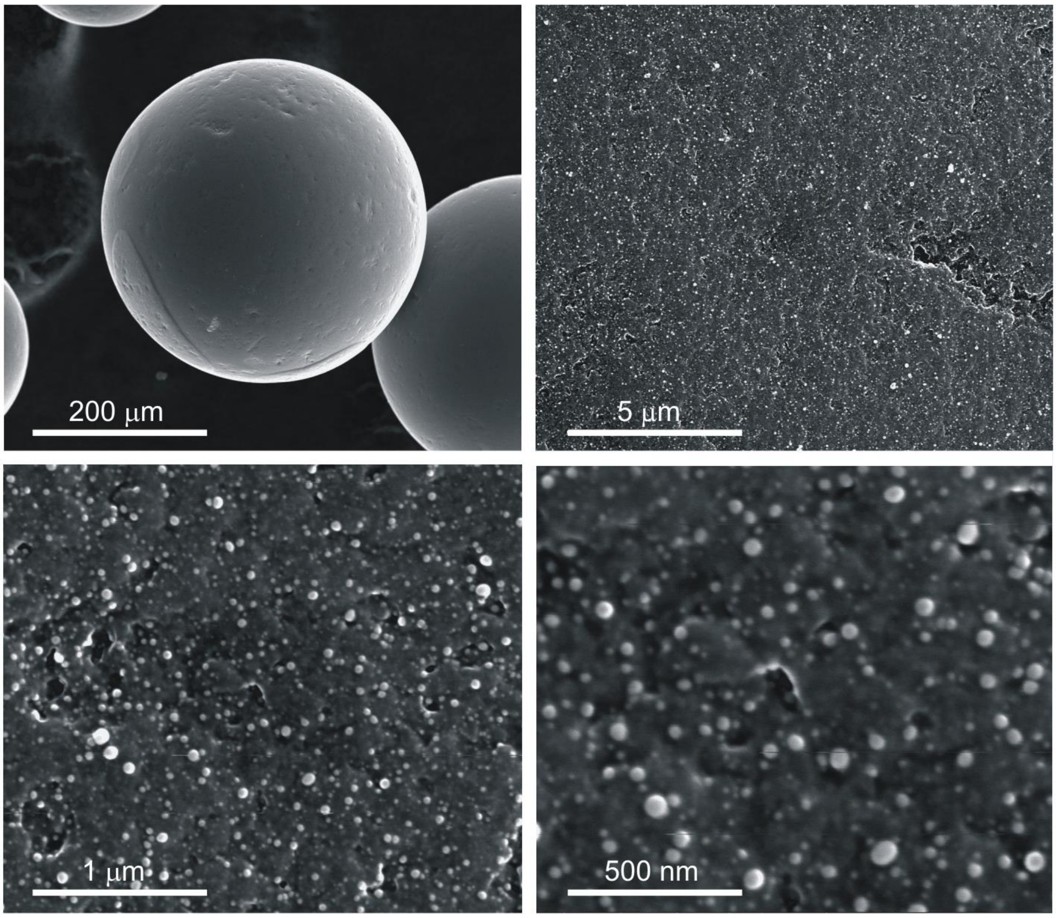

Figure S4. SEM images of the Cu-NP/C catalyst surface obtained by carbonisation of the copper-loaded ion-exchange resin at 600 ºC for 4 h

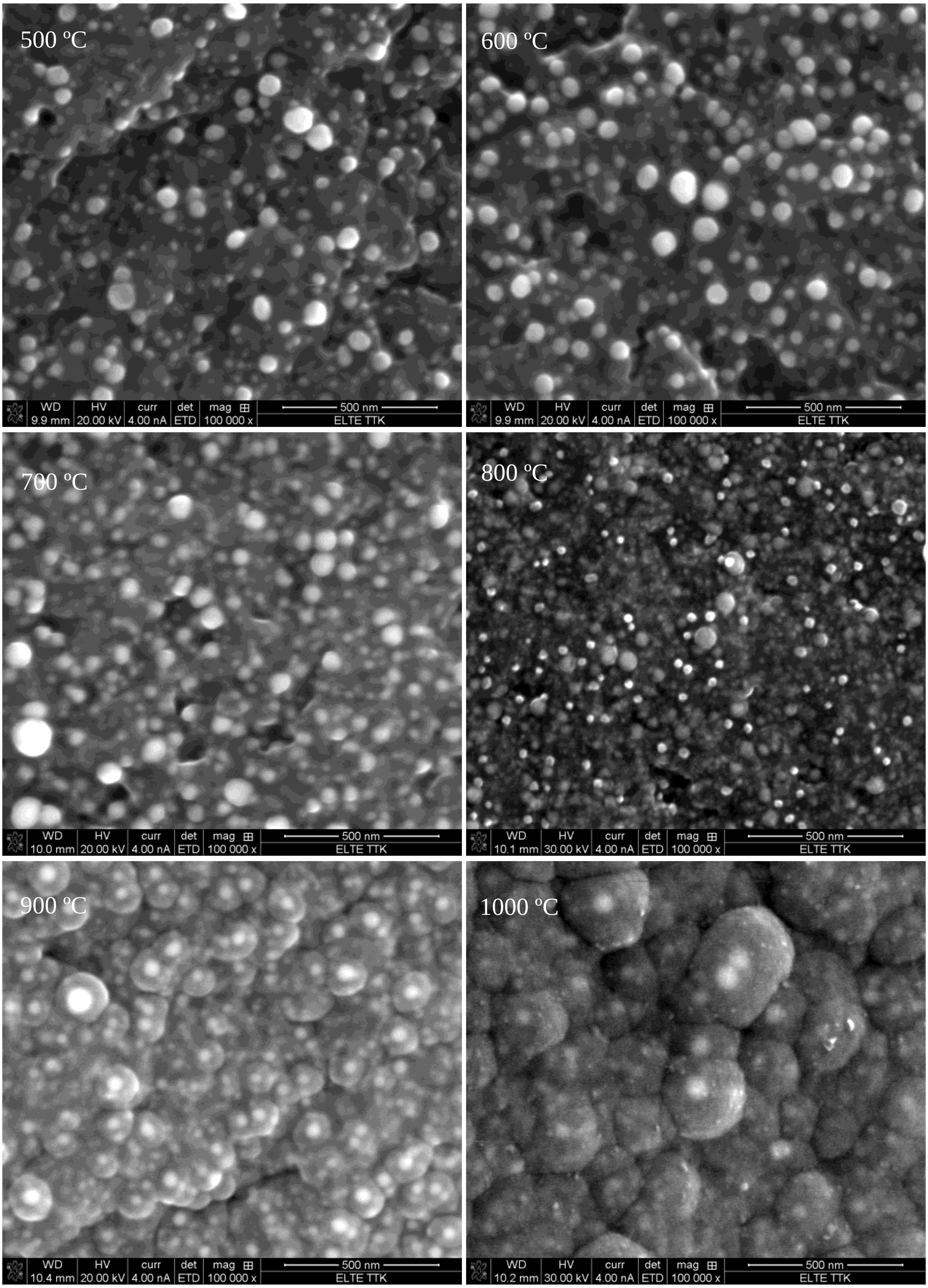

Figure S5. SEM images of Cu-NP/C microsphere surfaces obtained by carbonisation of the copper-loaded ion-exchange resin at 500 – 1000 ºC for 2 h

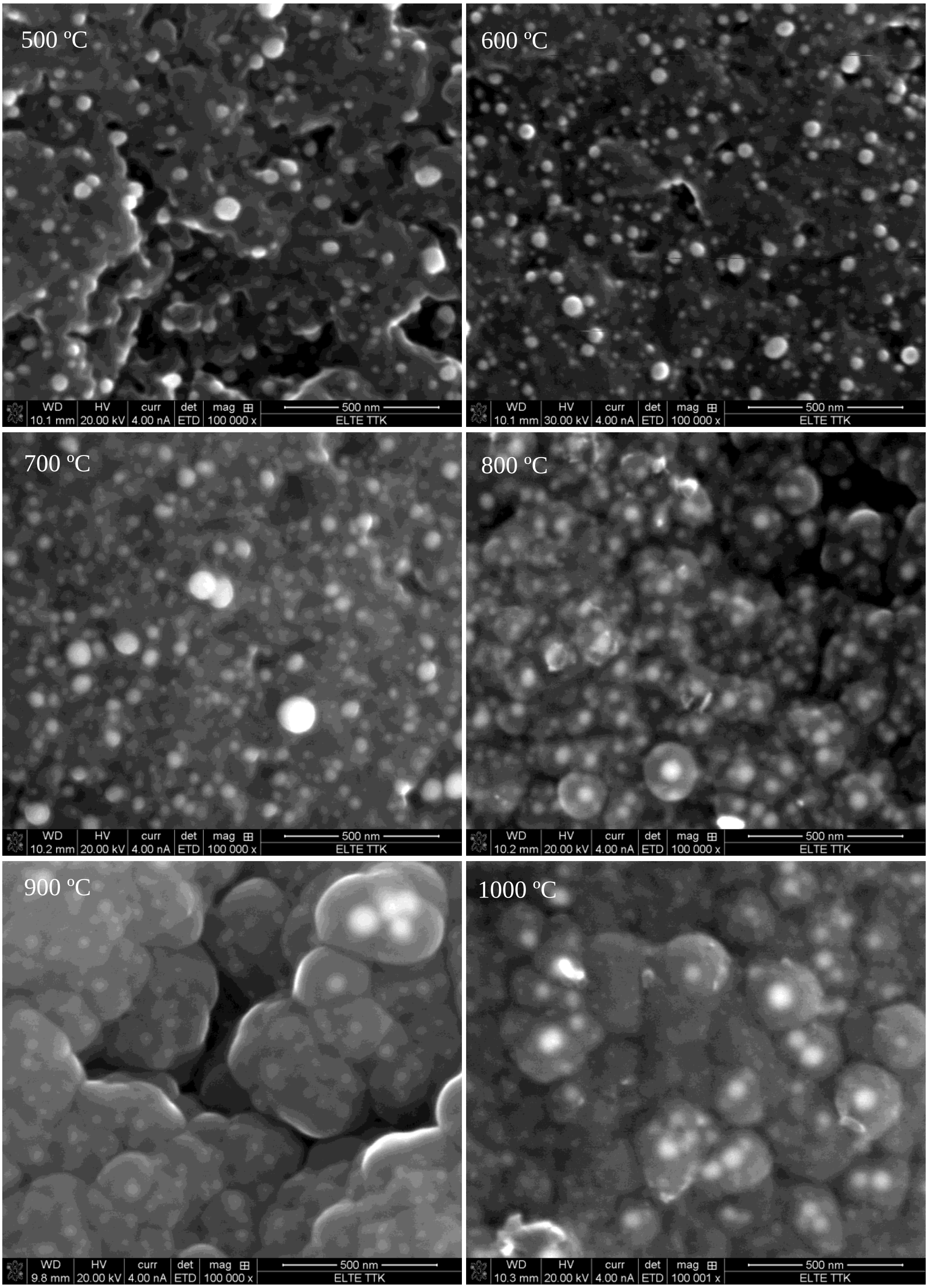

Figure S6. SEM images of Cu-NP/C microsphere surfaces obtained by carbonisation of the copper-loaded ion-exchange resin at 500 – 1000 ºC for 4 h

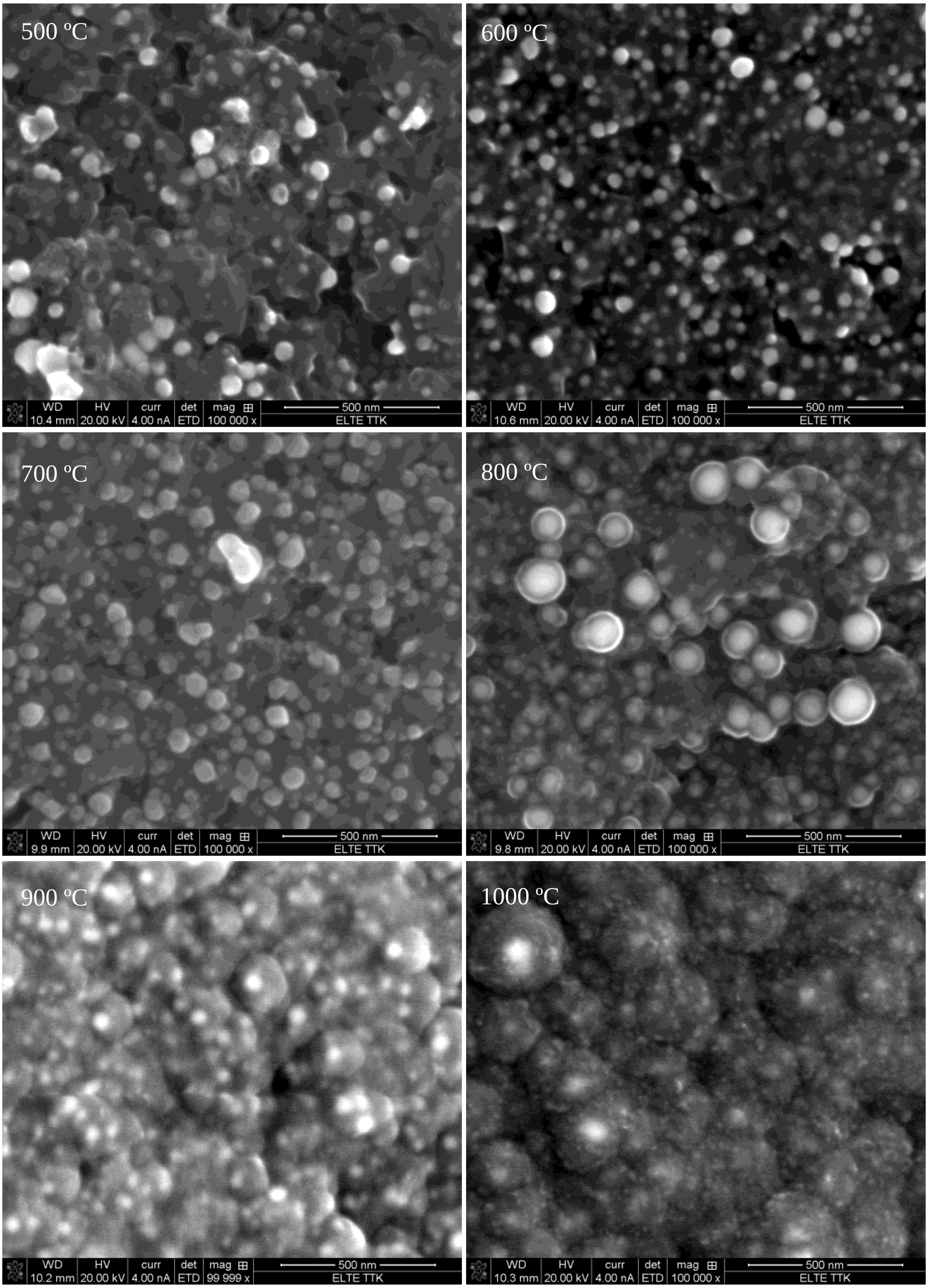

Figure S7. SEM images of Cu-NP/C microsphere surfaces obtained by carbonisation of the copper-loaded ion-exchange resin at 500 – 1000 ºC for 8 h

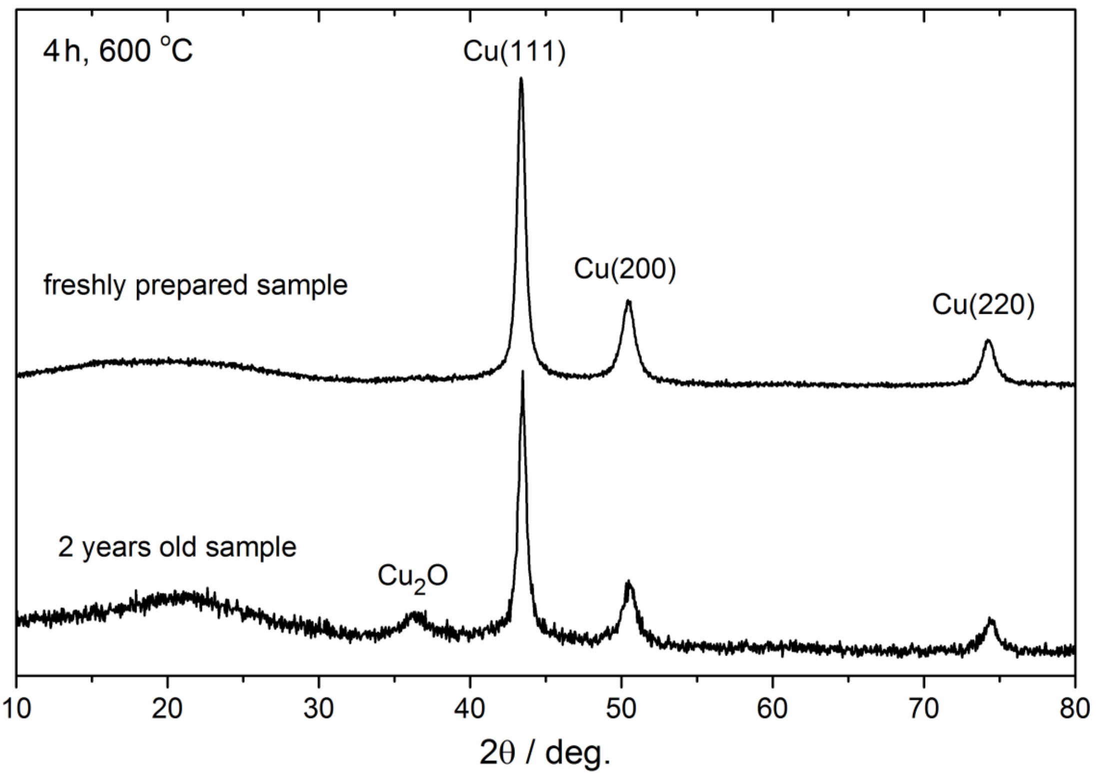

Figure S8. Powder X-ray diffractograms of a freshly prepared and 2 years old Cu-NP/C catalyst sample prepared by carbonisation of copper-loaded resin at 600 ºC for 4 h

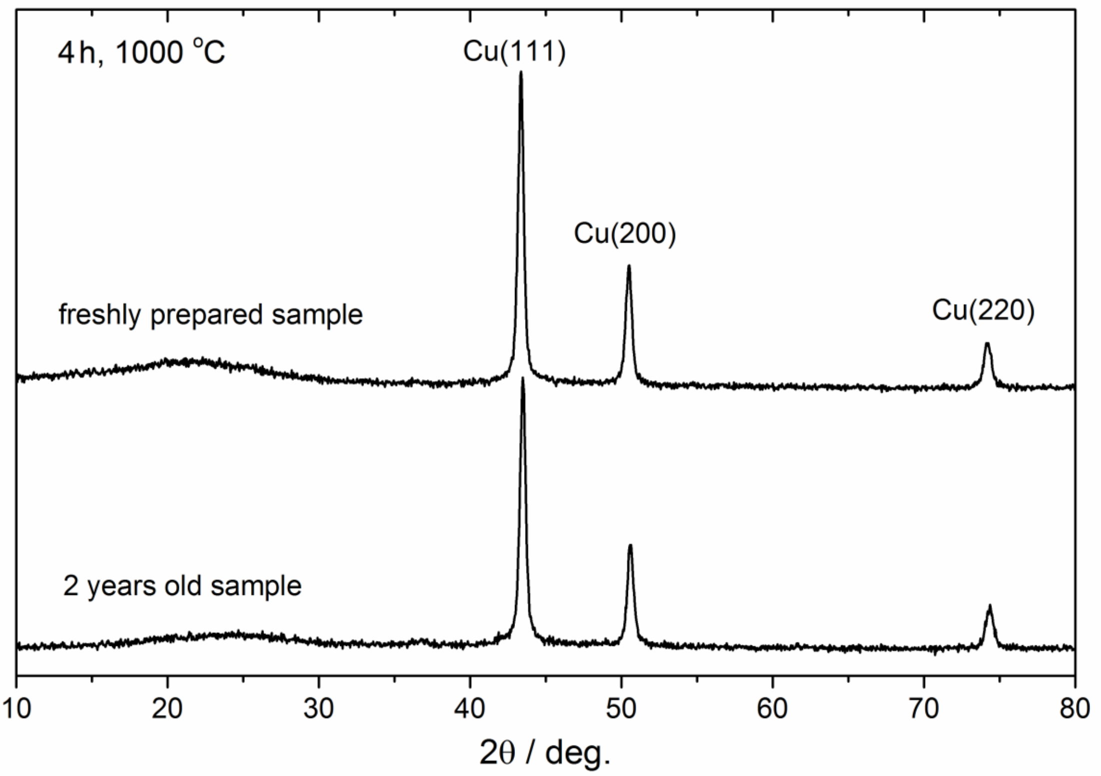

Figure S9. Powder X-ray diffractograms of a freshly prepared and 2 years old Cu-NP/C microsphere sample prepared by carbonisation of copper-loaded resin at 1000 ºC for 4 h

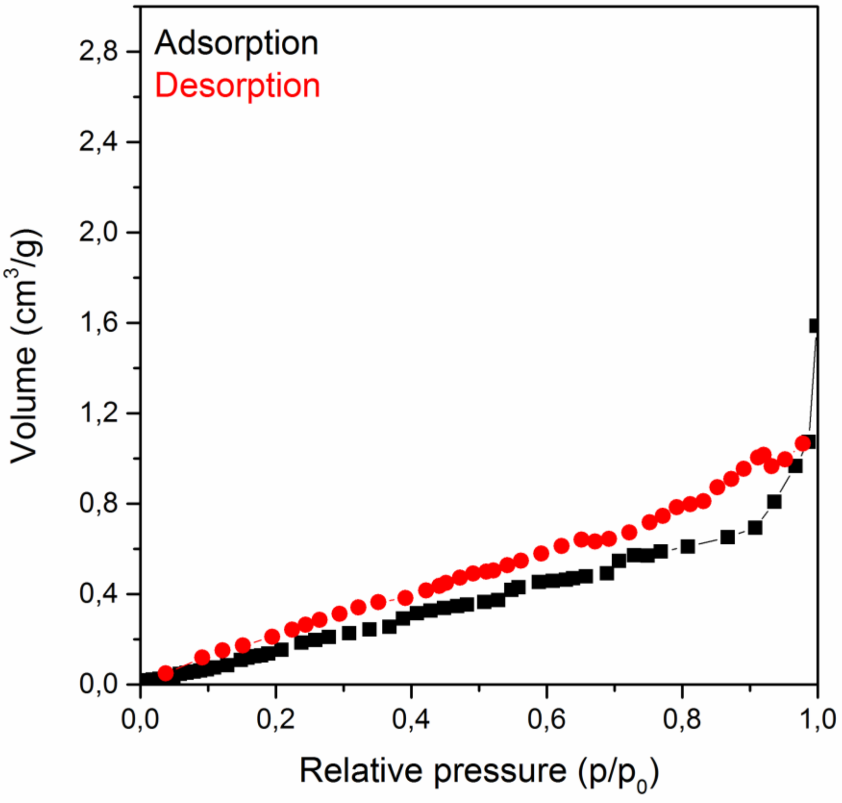

Figure S10. Nitrogen sorption isotherms of Cu-NP/C microsphere sample prepared by carbonisation of copper-loaded resin at 600 ºC for 4 h

Nitrogen sorption experiments were performed using Quantachrome Autosorb 1C static volumetric apparatus by measuring the increase of volume at equilibrium as a function of the relative pressure. Measurements were carried out at 77 K. The sample was outgassed prior to measurements at 300 °C for 24 h. Adsorption data were obtained using ca. 0.05 g of sample and successive doses of the selected gas until $p/p_0=1$ relative pressure was reached.

Total pore volume was obtained to be $1.666 \cdot 10^{-3}$ cm^{3}g^{-1} at $p/p_0=0.98702$. Calculated average pore width (D) was estimated to be 2.2 nm using the equation of D= 4V/S (V is the total pore volume and S is the specific surface area). The nitrogen isotherms suggest poorly developed micro- and mesopores.

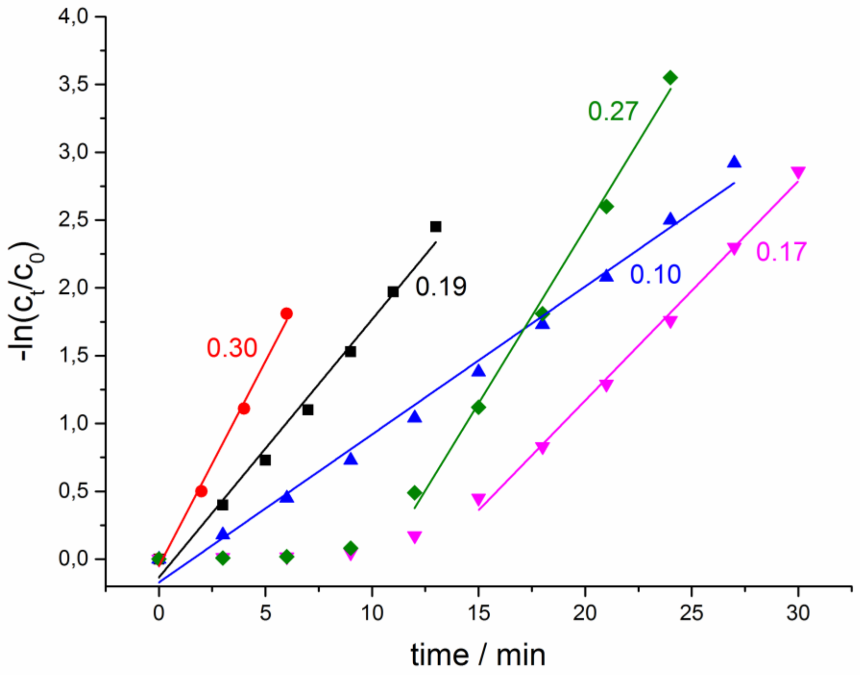

Figure S11. Plot of –ln(c_t/c_0) vs. time for the reduction of 4NP to 4AP (c is the concentration of 4NP). Slope of fitted lines are indicated. The ratio of the rate constant over the total weight of the catalyst (k_{app}/m_{cat})= 75, 95, 100, 68, 85 $min^{-1}g^{-1}$. Cu-NP/C microspheres prepared by carbonisation at 600 °C for 4 h are used.

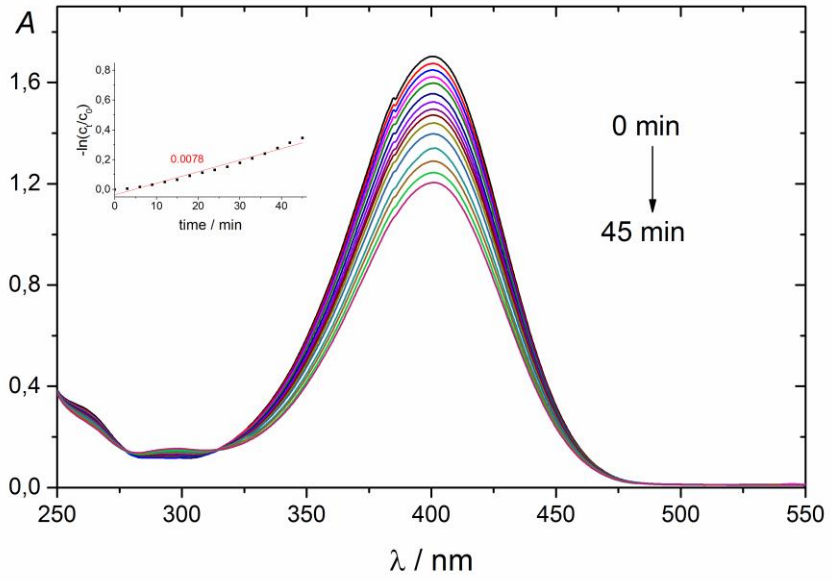

Figure S12. Time dependent evolution of UV/Vis spectra of 4NP anion at the presence of Cu-NP/C microspheres prepared by carbonisation at 1000 °C for 4 h. Insert shows plot of –ln(c_t/c_0) vs. time. Slope of fitted line is indicated. k_{app}/m_{cat}= 3.9 $min^{-1}g^{-1}$.

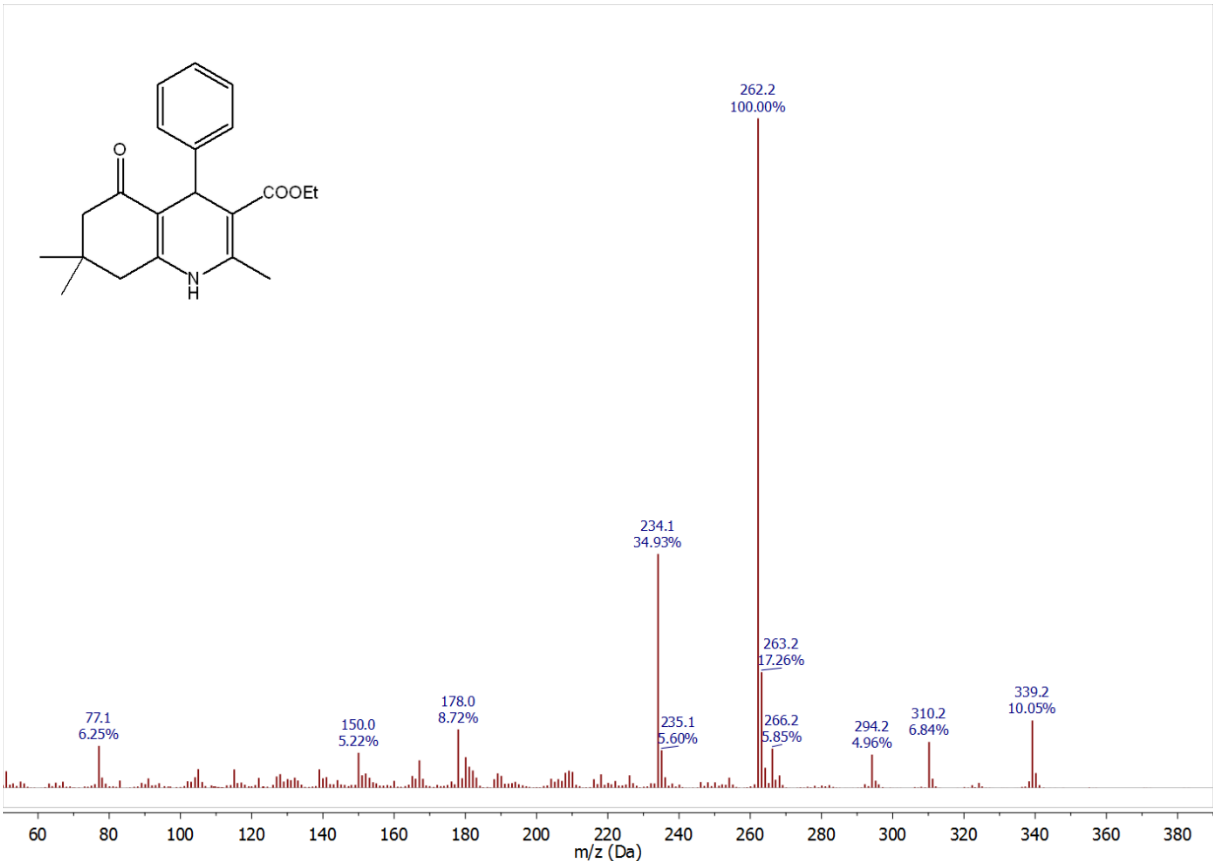

Figure S13. Mass spectrum of the phenyl-derivative recorded by using an Agilent 5973 Mass spectrometer of a GC-MS instrument (solvent: dichloromethane; carrier gas: He).

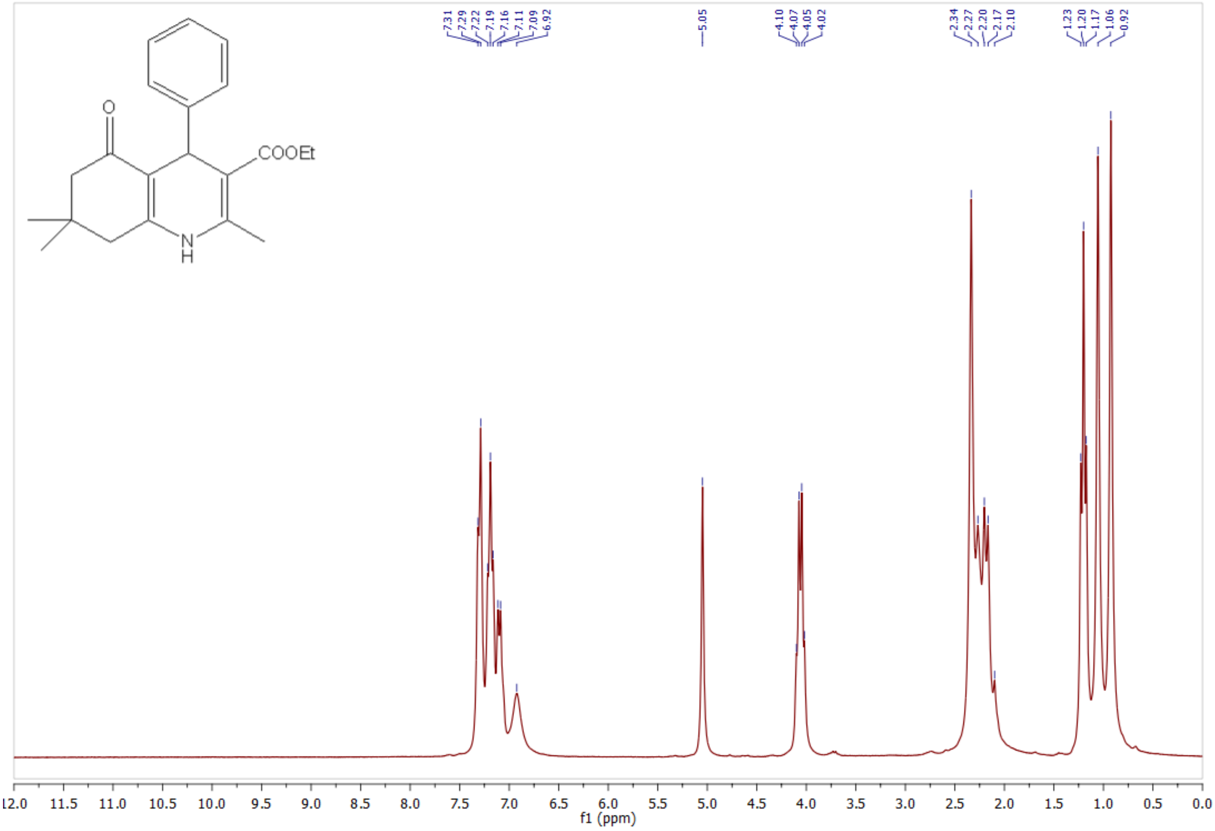

Figure S14. ^{1}H-NMR spectrum of the phenyl-derivative recorded in $CDCl_3$ at room temperature.

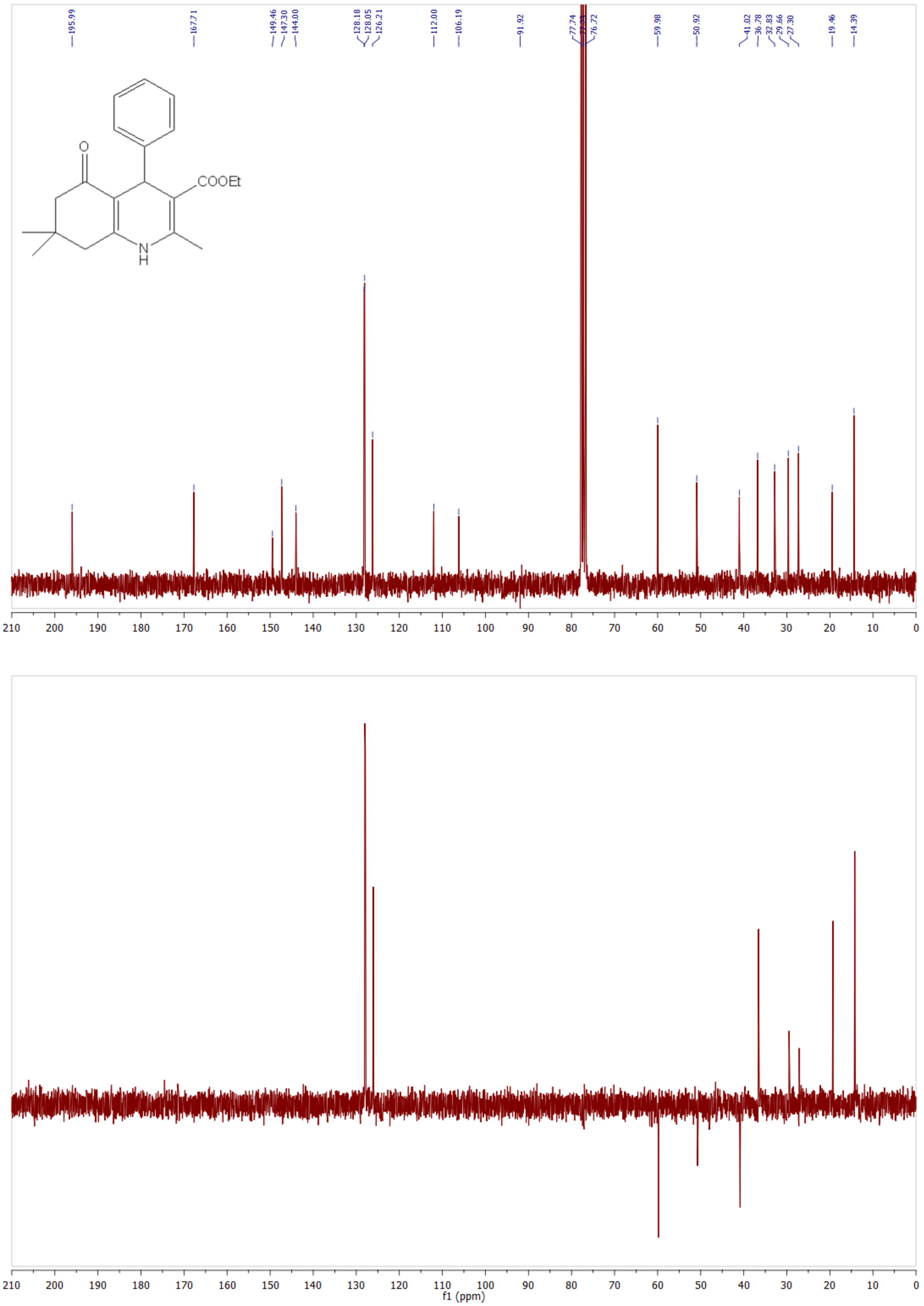

Figure S15. ^{13}C-NMR (top) and DEPT (bottom) spectra of the phenyl-derivative recorded in $CDCl_3$ at room temperature.

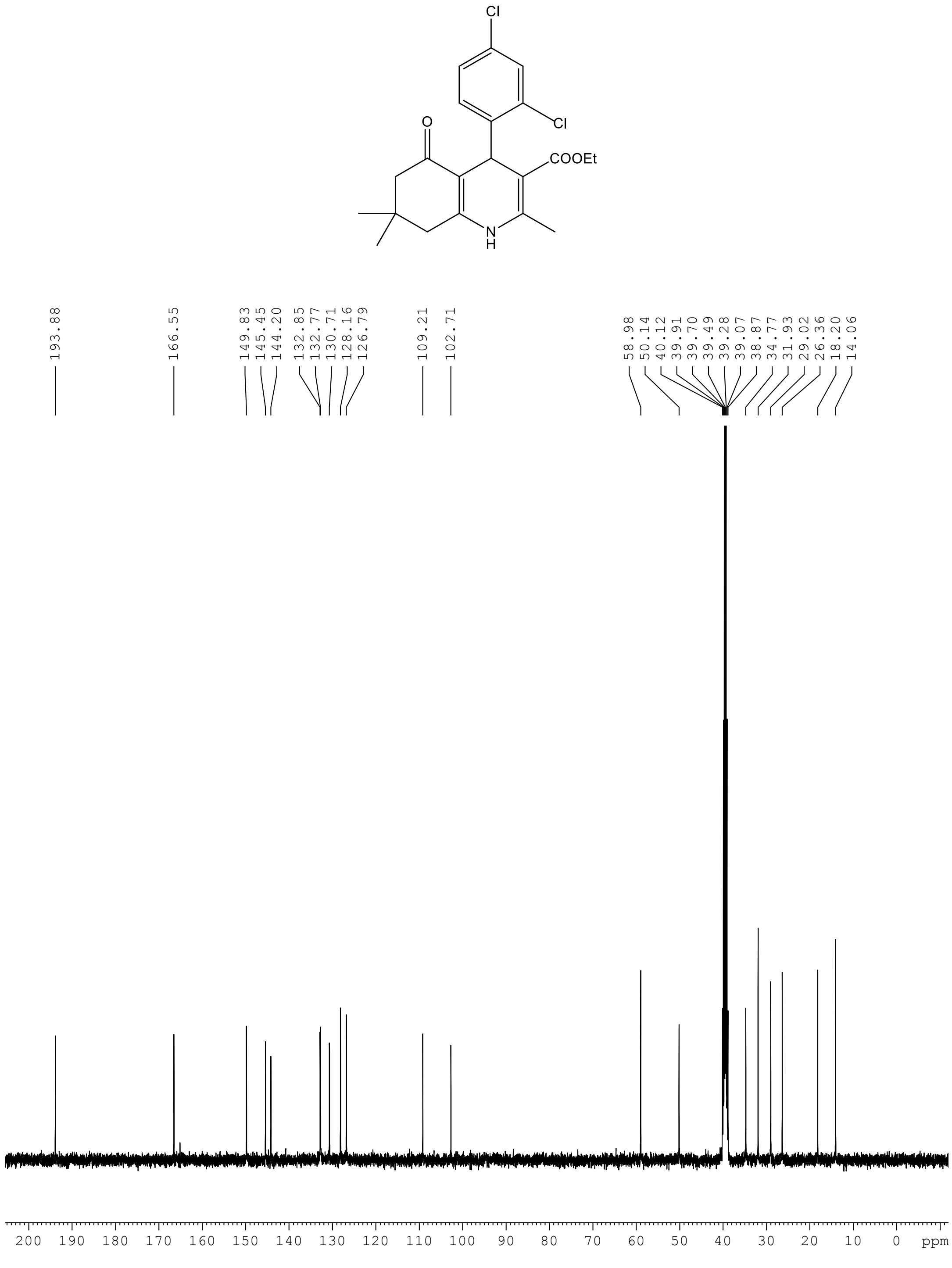

Figure S16. ^{13}C-NMR spectrum of the 2,4-dichlorophenyl-derivative recorded in DMSO-d_6 at room temperature.

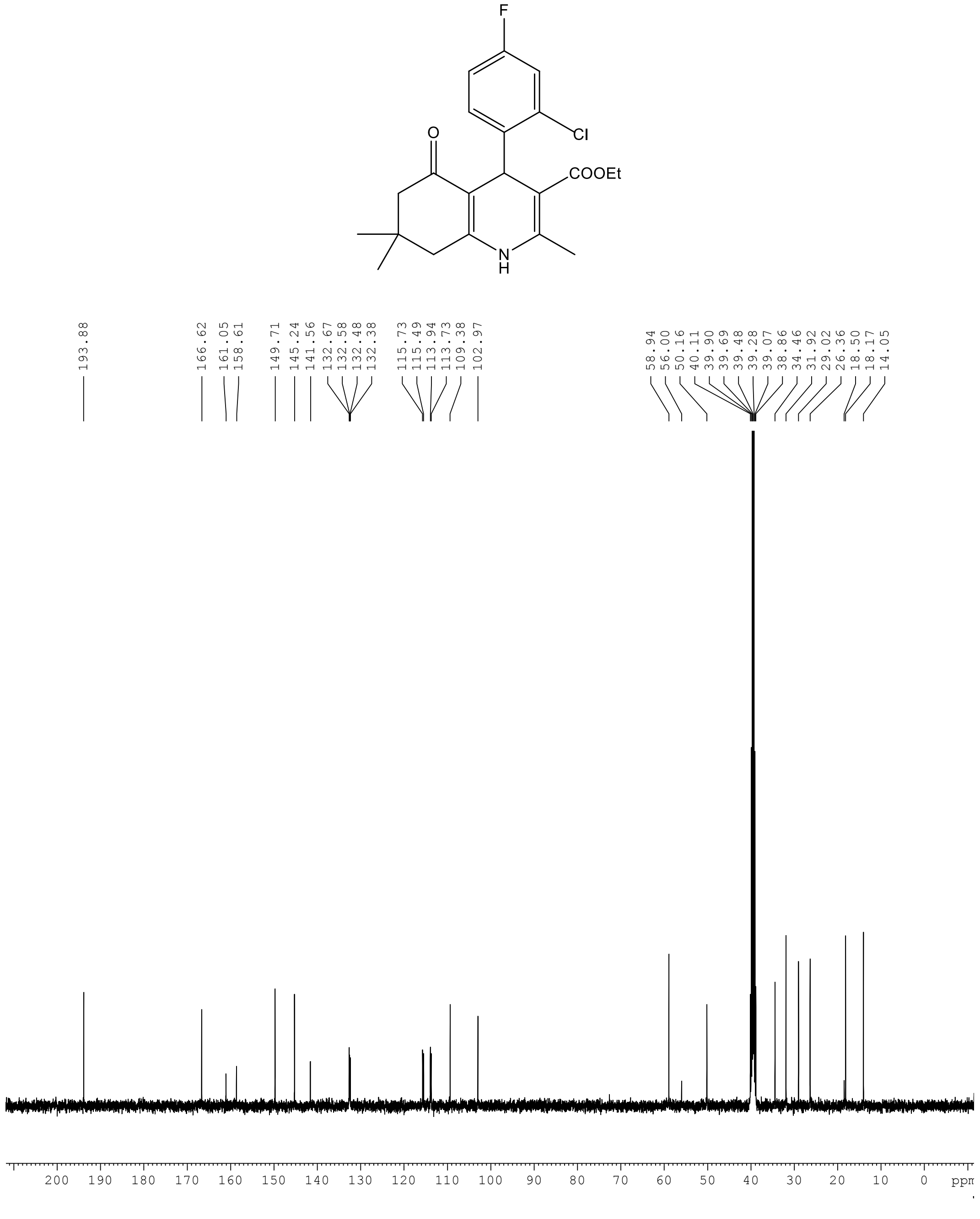

Figure S17. ^{13}C-NMR spectrum of the 2-chloro-4-fluorophenyl-derivative recorded in DMSO-d_6 at room temperature.

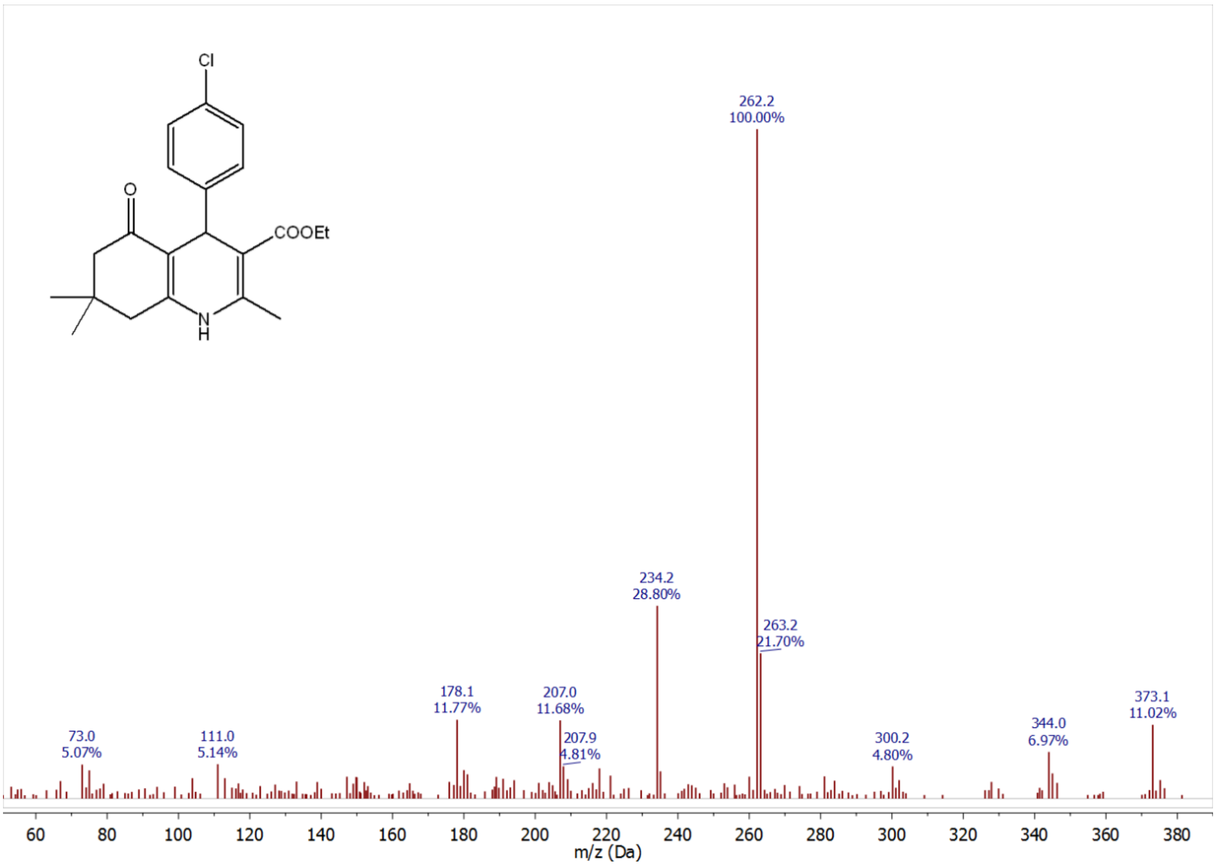

Figure S18. Mass spectrum of the 4-chlorophenyl-derivative recorded by using an Agilent 5973 Mass spectrometer of a GC-MS instrument (solvent: dichloromethane; carrier gas: He).

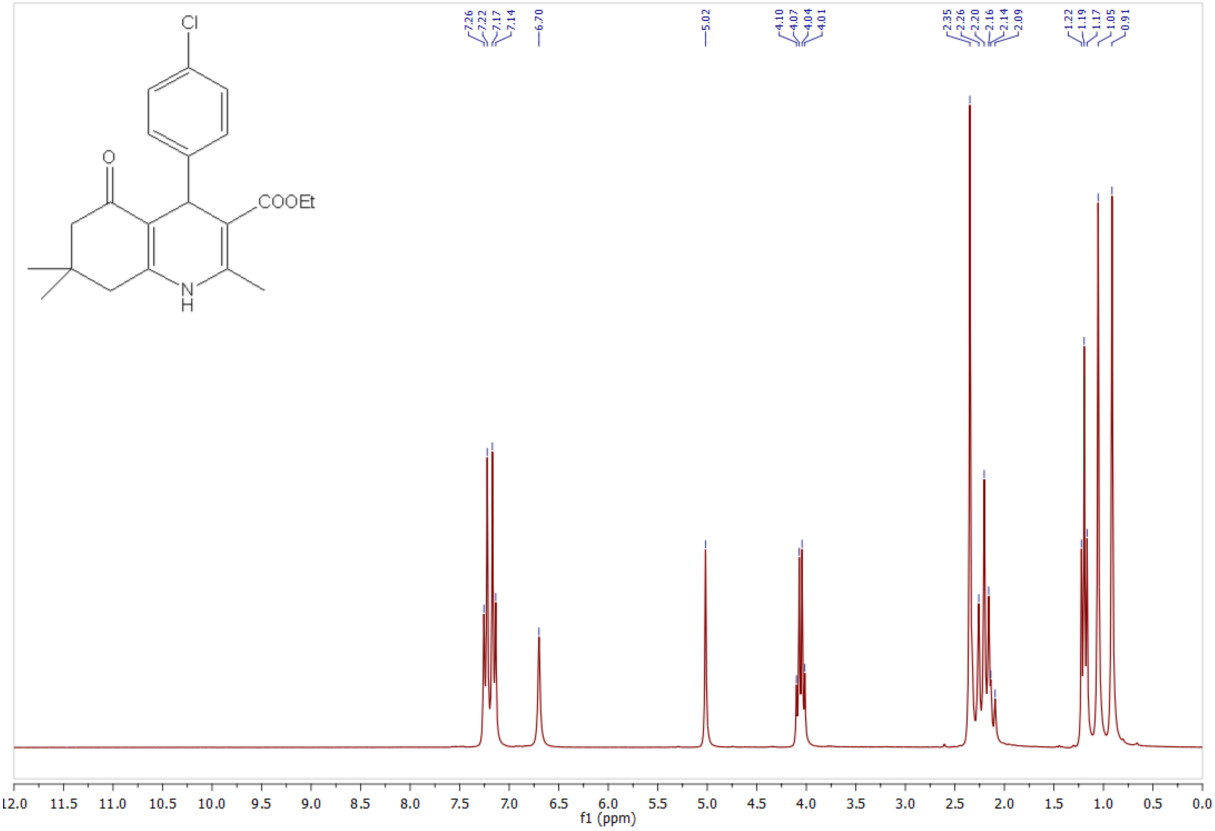

Figure S19. ^{1}H-NMR spectrum of the 4-chlorophenyl-derivative recorded in $CDCl_3$ at room temperature.

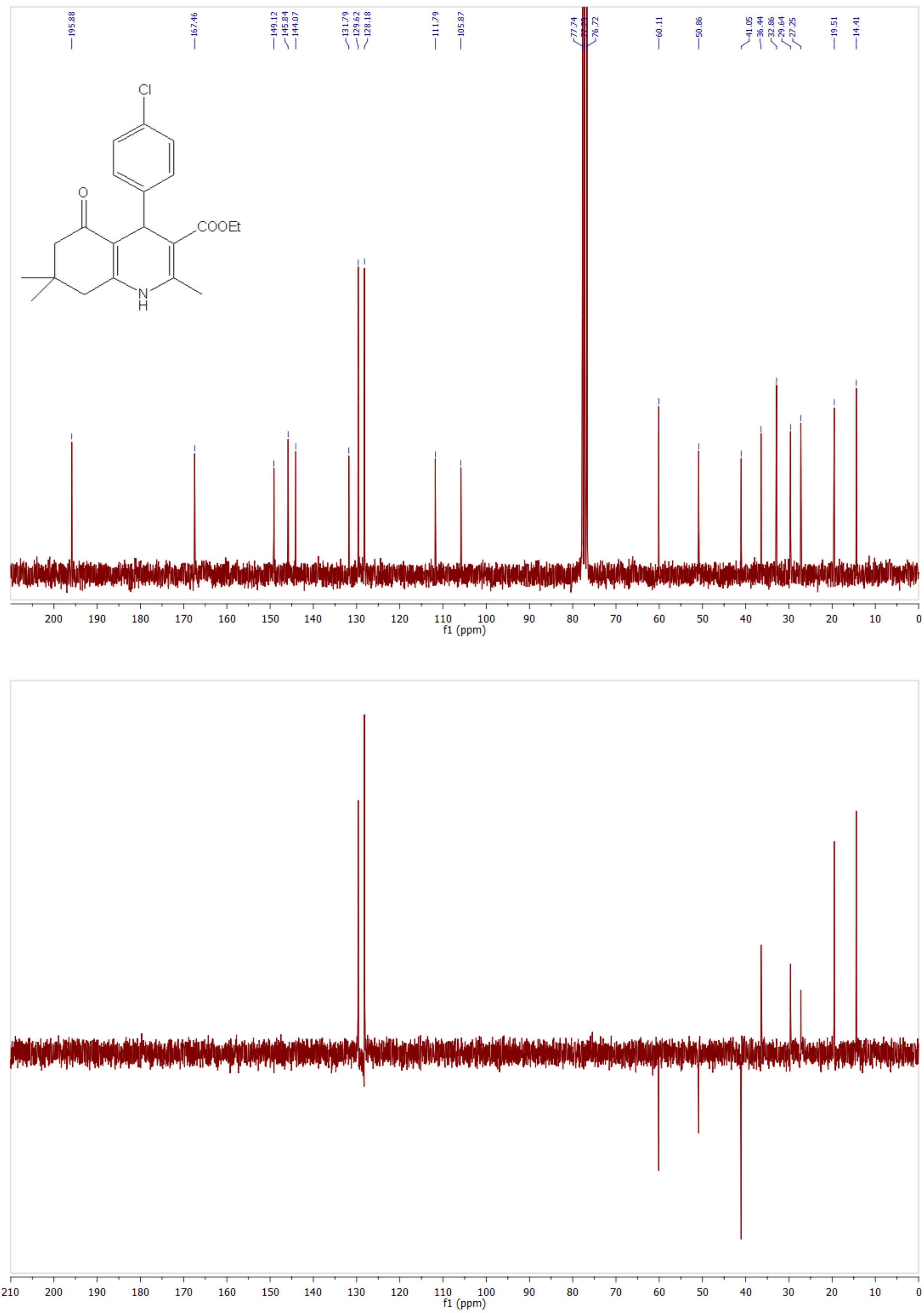

Figure S20. ^{13}C-NMR (top) and DEPT (bottom) spectra of the 4-chlorophenyl-derivative recorded in $CDCl_3$ at room temperature.

Figure S21. ^{13}C-NMR spectrum of the 2-fluorene-derivative recorded in DMSO-d_6 at room temperature.

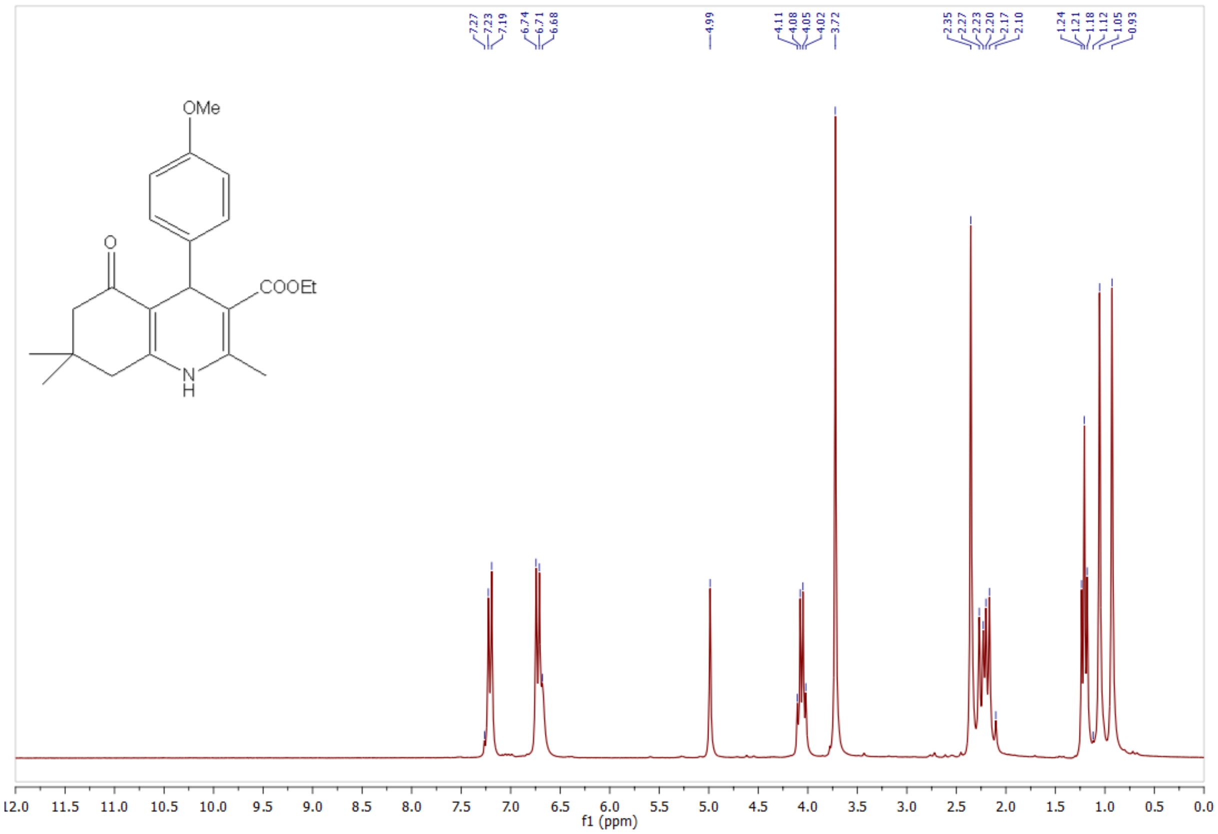

Figure S22. ^{1}H-NMR spectrum of the 4-methoxyphenyl-derivative recorded in $CDCl_3$ at room temperature.

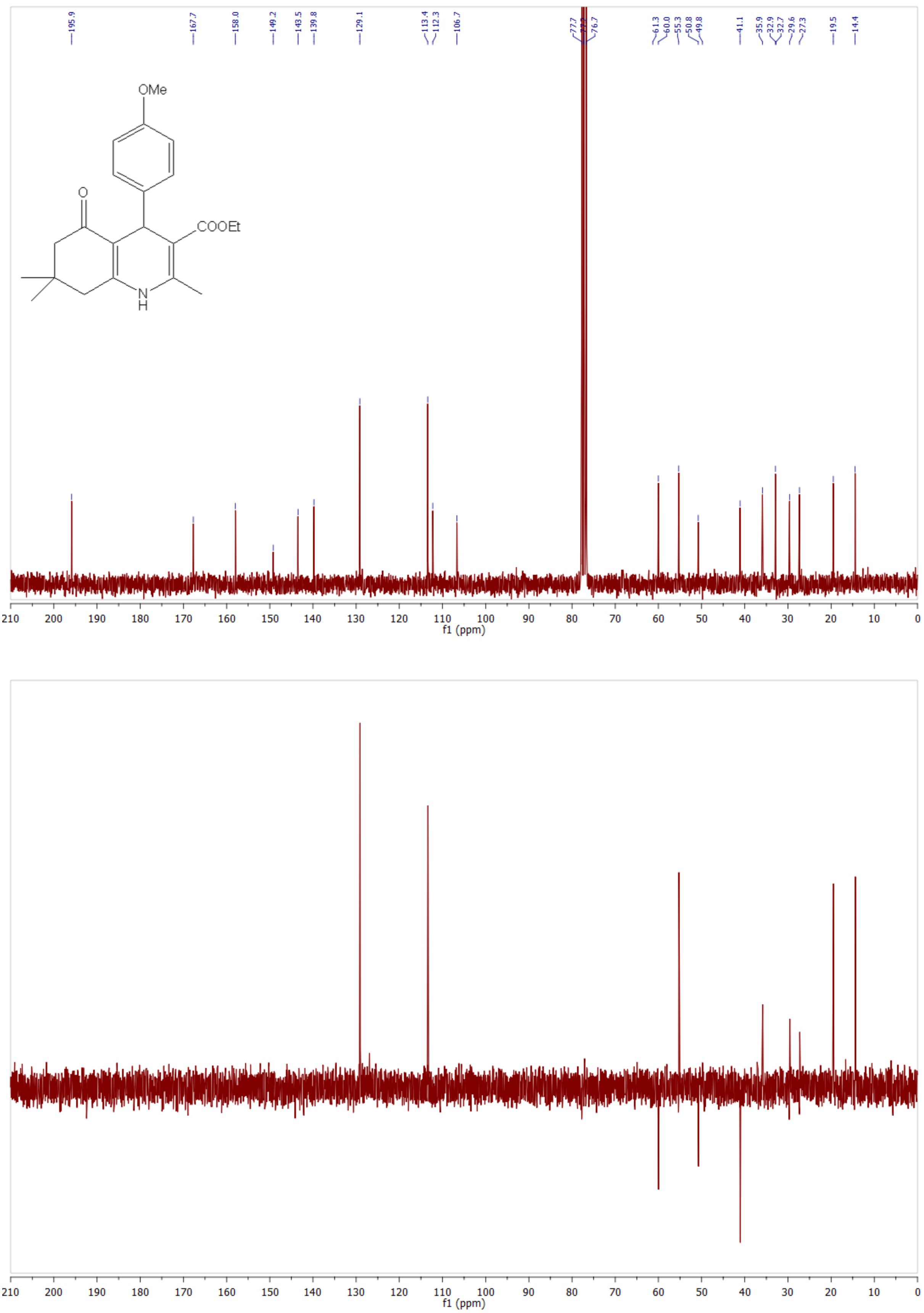

Figure S23. ^{13}C-NMR (top) and DEPT (bottom) spectra of the 4-methoxyphenyl-derivative recorded in $CDCl_3$ at room temperature.

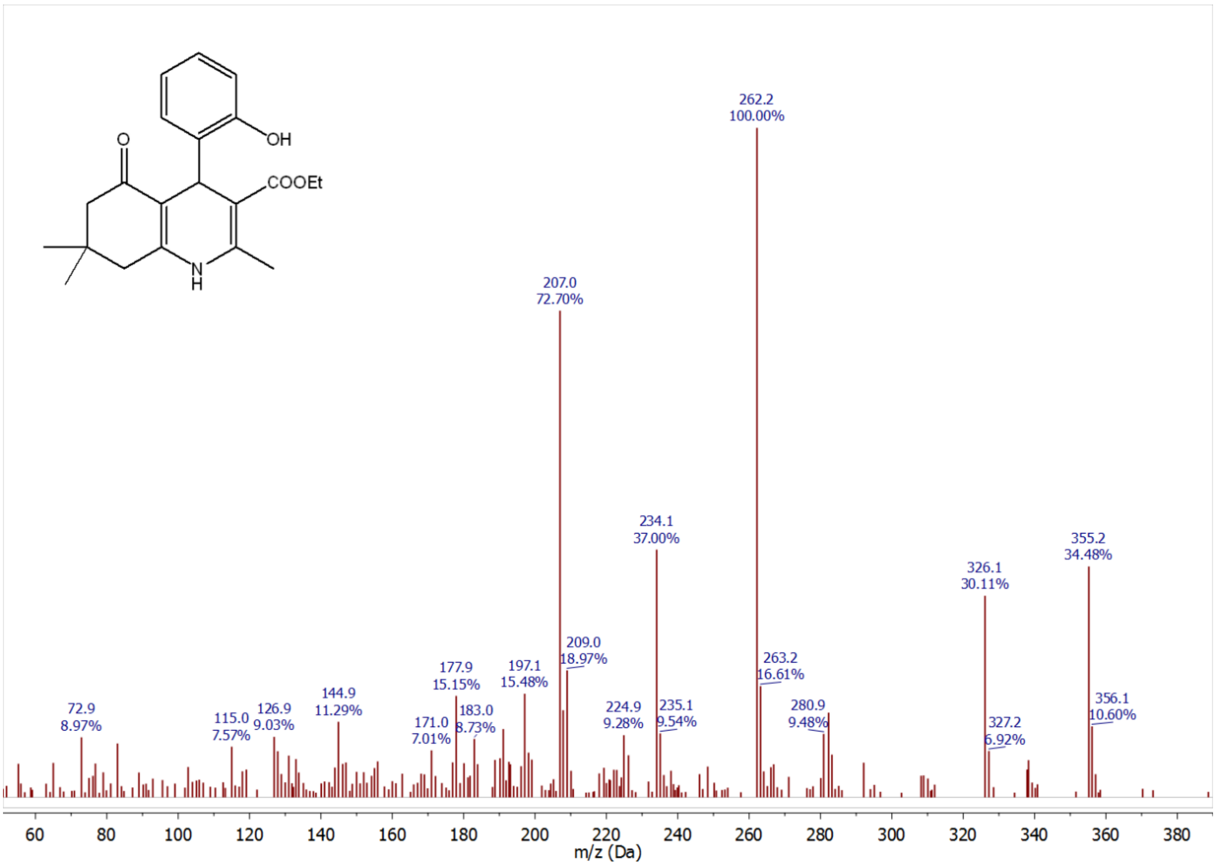

Figure S24. Mass spectrum of the 2-hydroxyphenyl-derivative recorded by using an Agilent 5973 Mass spectrometer of a GC-MS instrument (solvent: dichloromethane; carrier gas: He).

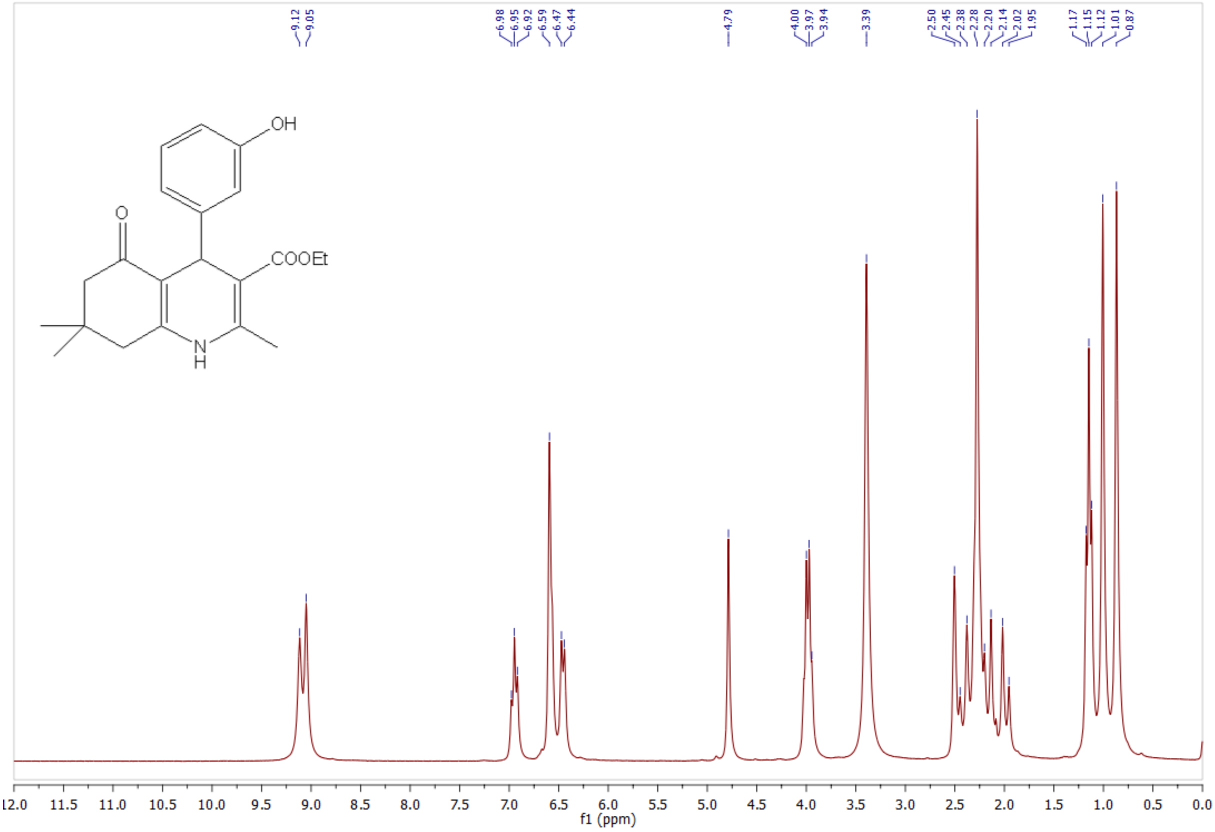

Figure S25. ^{1}H-NMR spectrum of the 3-hydroxyphenyl-derivative recorded in DMSO-d_6 at room temperature. Large peak at 3.39 ppm is due to water impurity.

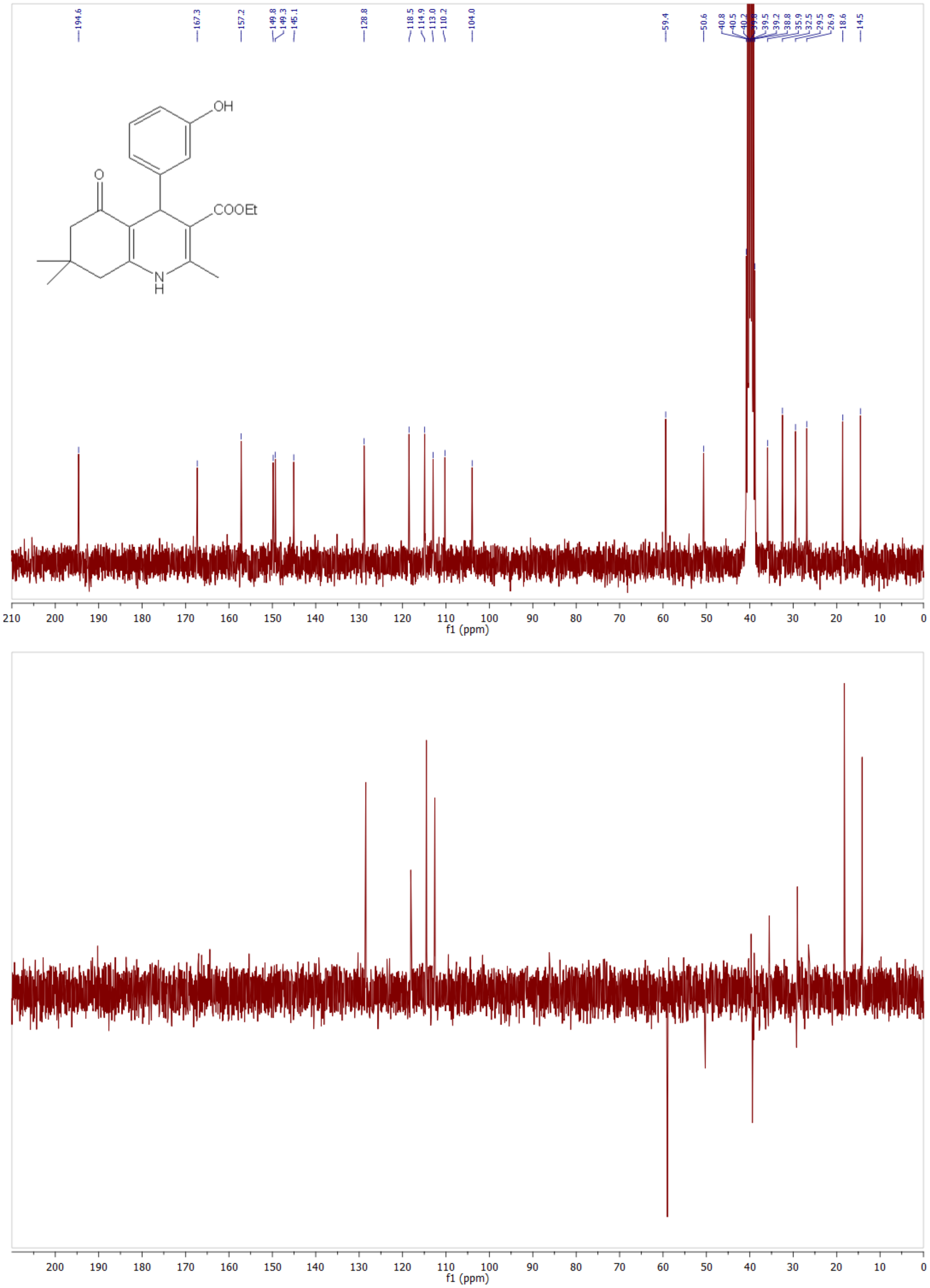

Figure S26. ^{13}C-NMR (top) and DEPT (bottom) spectra of the 3-hydroxyphenyl-derivative recorded in DMSO-d$_6$ at room temperature.

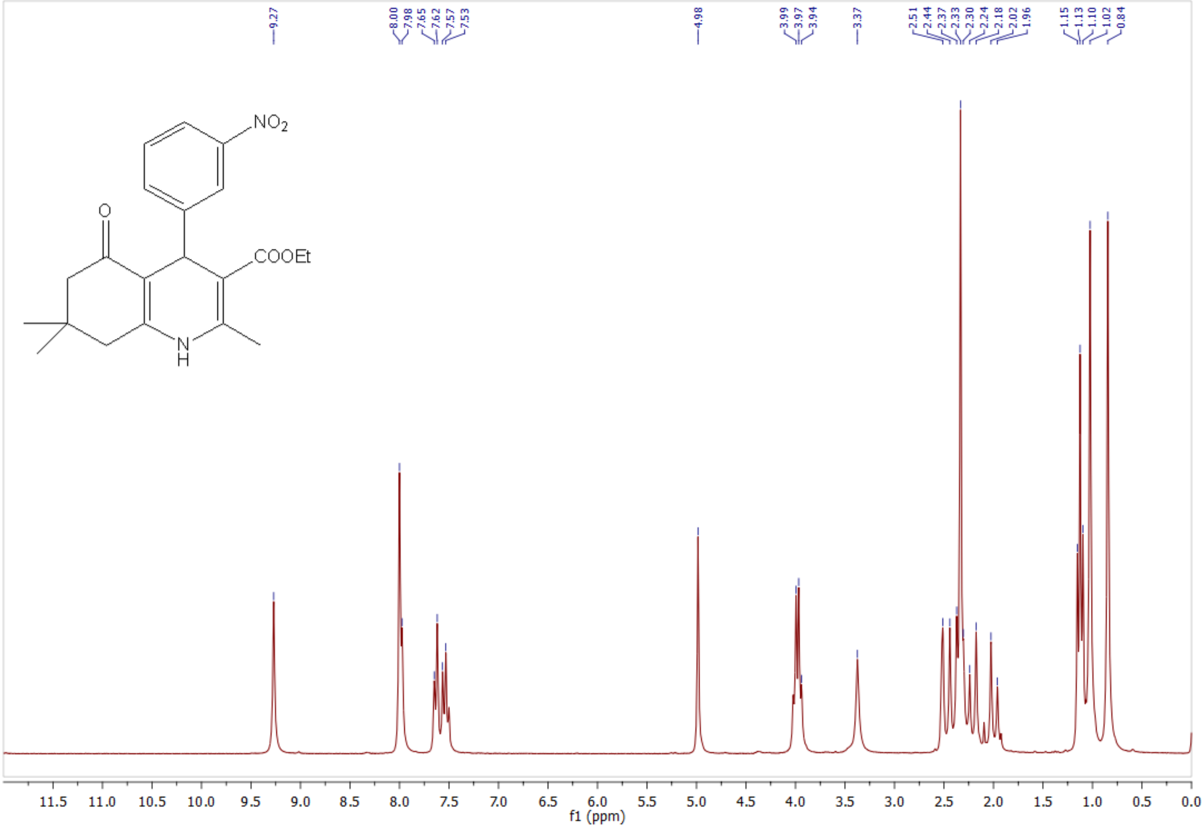

Figure S27. ^{1}H-NMR spectrum of the 3-nitrophenyl-derivative recorded in DMSO-d_6 at room temperature. Peak at 3.37 ppm is due to water impurity.

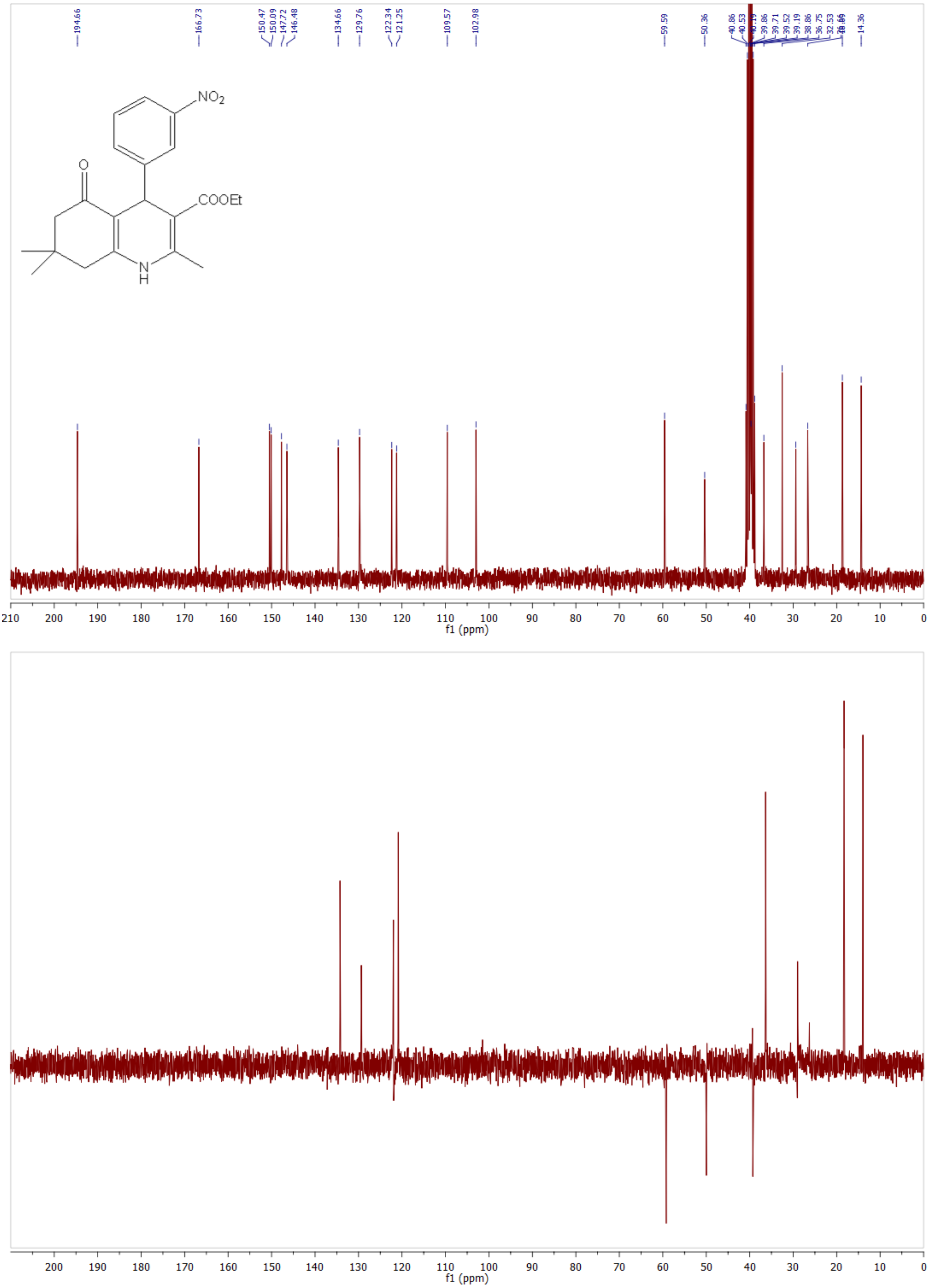

Figure S28. ^{13}C-NMR (top) and DEPT (bottom) spectra of the 3-nitrophenyl-derivative recorded in DMSO-d_6 at room temperature.

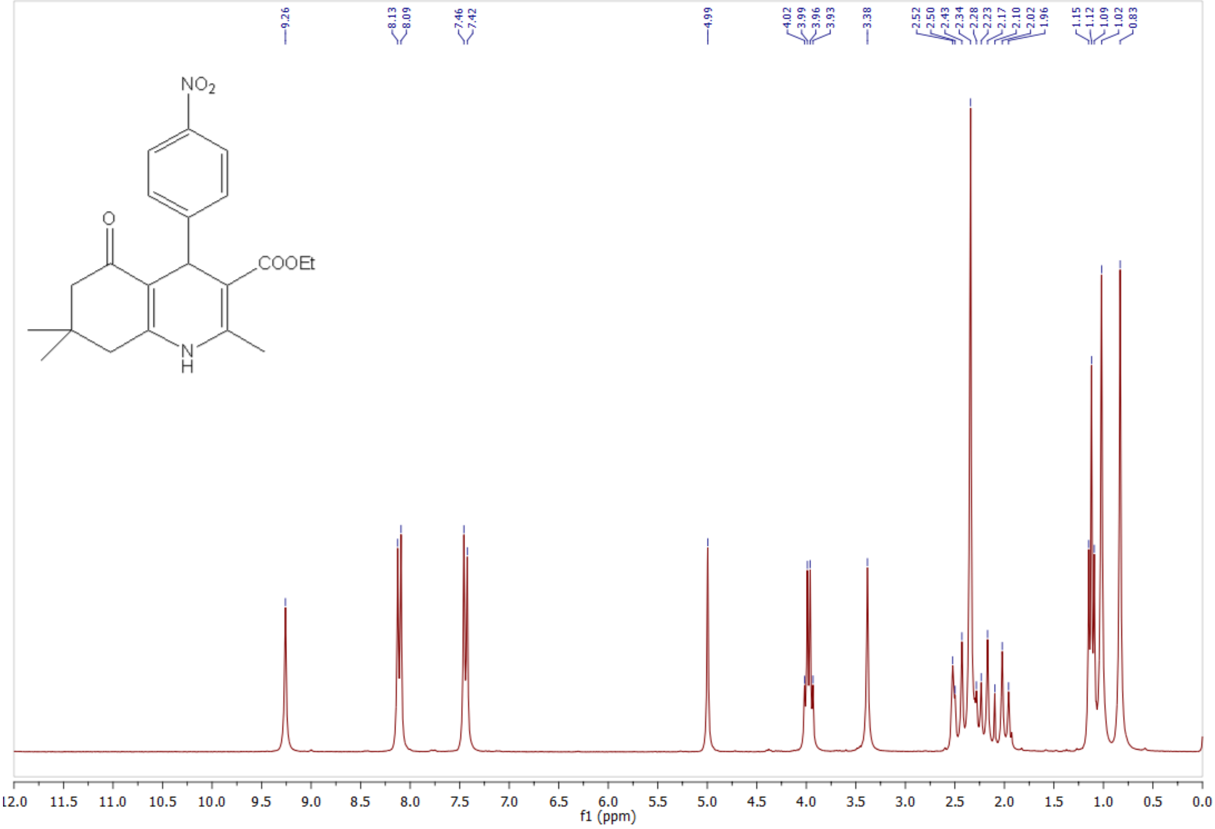

Figure S29. ^{1}H-NMR spectrum of the 4-nitrophenyl-derivative recorded in DMSO-d_6 at room temperature. Peak at 3.38 ppm is due to water impurity.

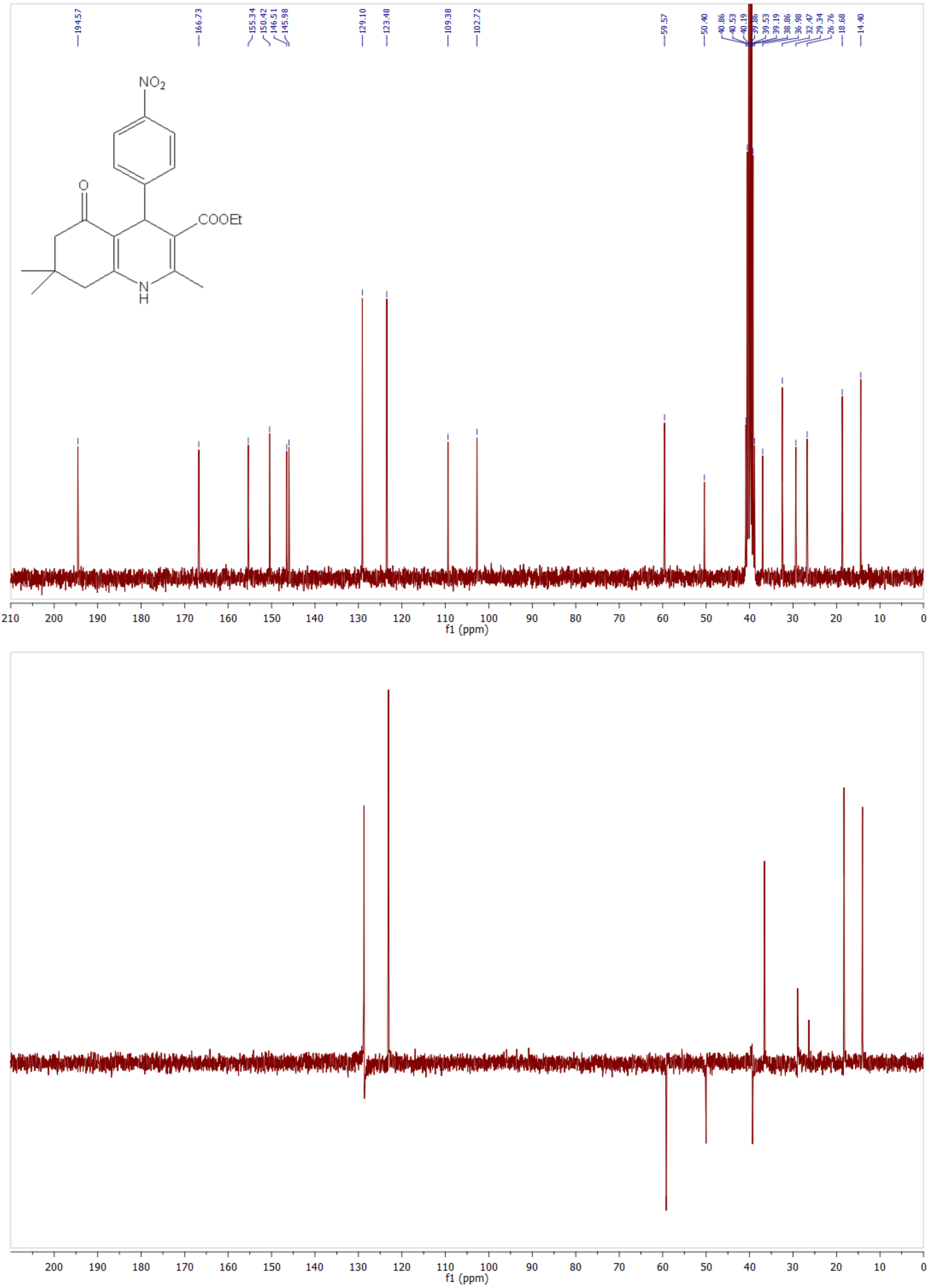

Figure S30. ^{13}C-NMR (top) and DEPT (bottom) spectra of the 4-nitrophenyl-derivative recorded in DMSO-d_6 at room temperature.

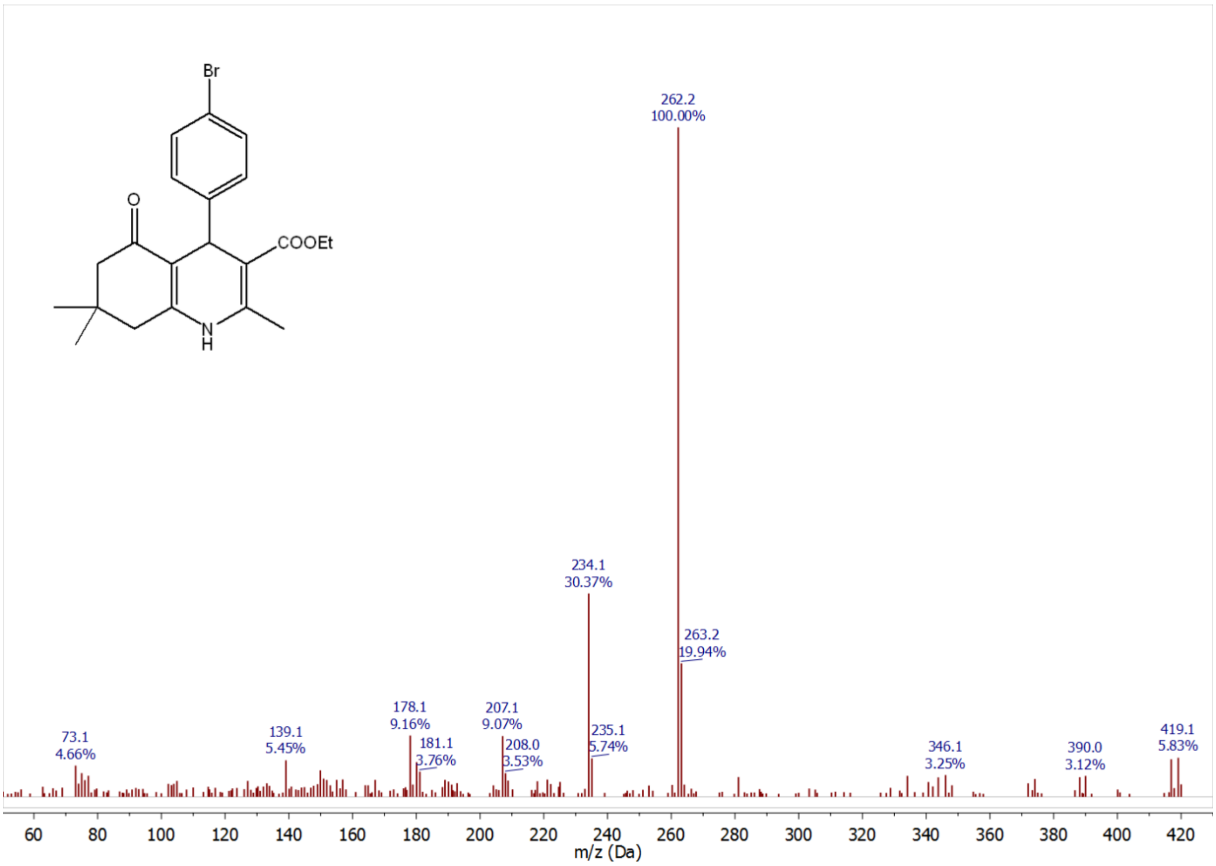

Figure S31. Mass spectrum of the 4-bromophenyl-derivative recorded by using an Agilent 5973 Mass spectrometer of a GC-MS instrument (solvent: dichloromethane; carrier gas: He).

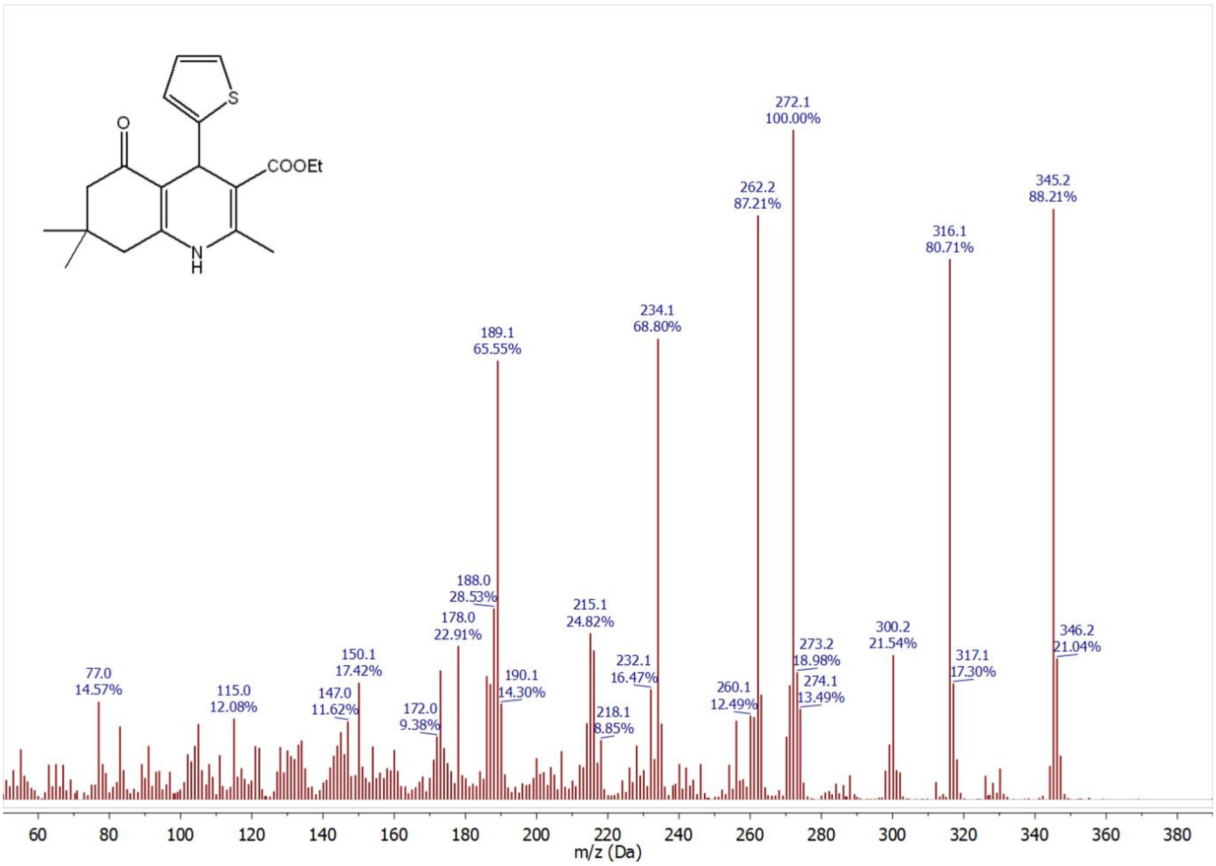

Figure S32. Mass spectrum of the 2-thiophenyl-derivative recorded by using an Agilent 5973 Mass spectrometer of a GC-MS instrument (solvent: dichloromethane; carrier gas: He).

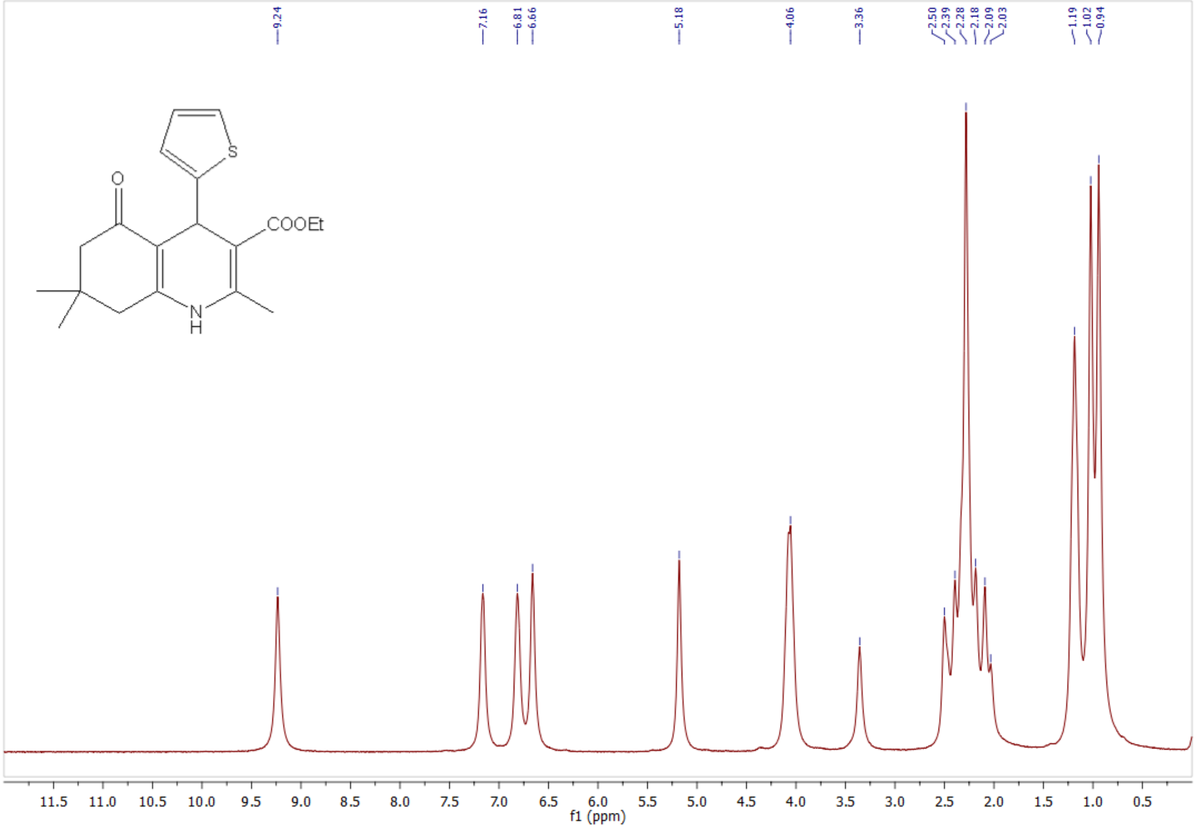

Figure S33. ^{1}H-NMR spectrum of the 2-thiophenyl-derivative recorded in DMSO-d_6 at room temperature. Peak at 3.36 ppm is due to water impurity.

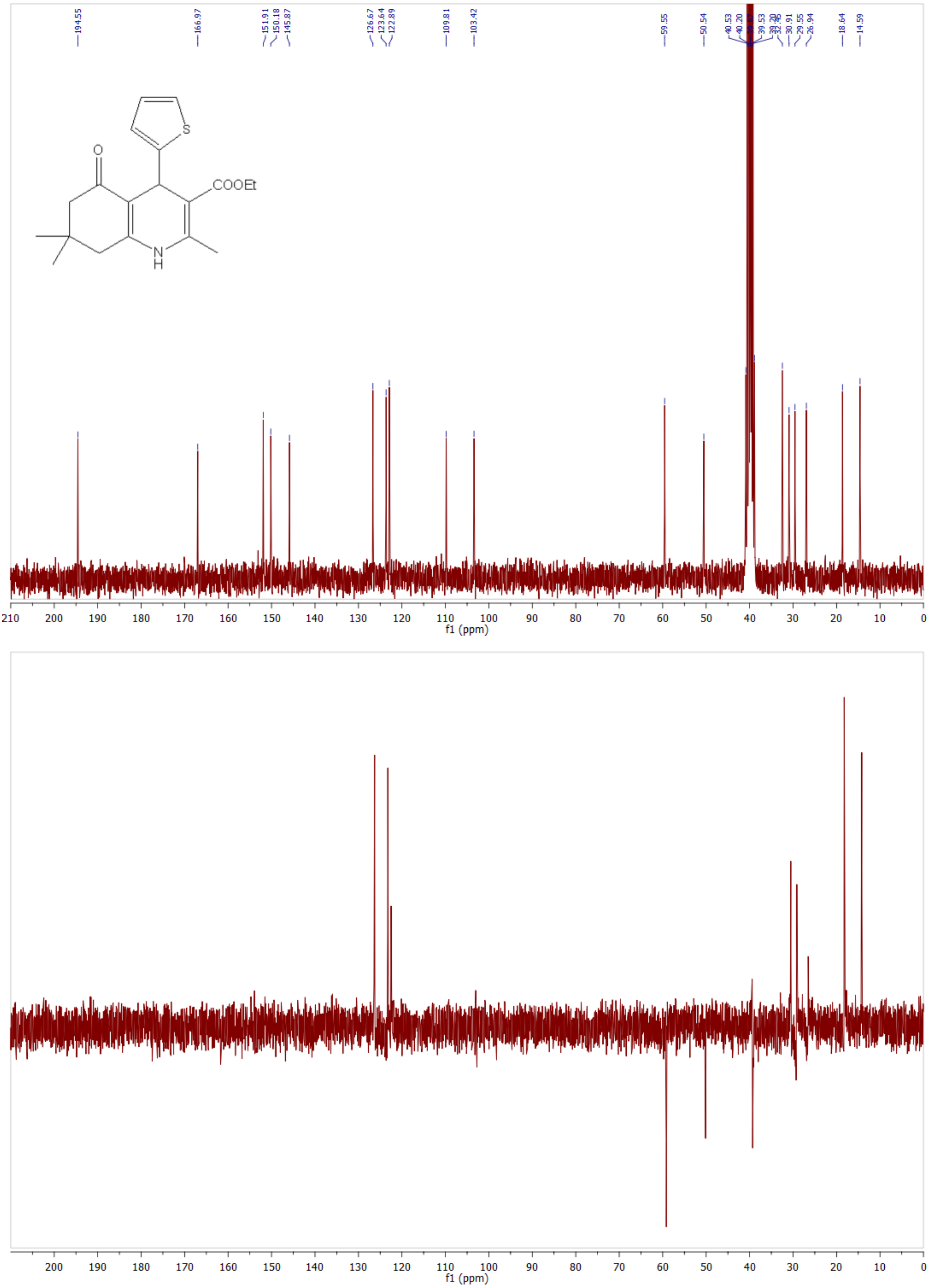

Figure S34. ^{13}C-NMR (top) and DEPT (bottom) spectra of the 2-thiophenyl-derivative recorded in DMSO-d_6 at room temperature.